

Fabrication of Superconducting Thin films and One-Probe T_c Measurements

Sonell Malik

*A dissertation submitted for the partial fulfilment of BS-MS dual
degree in Science*



Indian Institute of Science Education and Research, Mohali

May 24, 2021

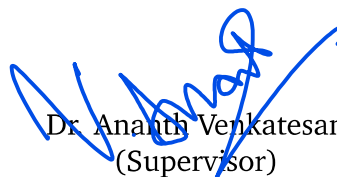
Certificate of Examination

This is to certify that the dissertation titled “Superconducting Thin Films” submitted by Sonell Malik (Reg. No. MS16066) for the partial fulfilment of BS-MS dual degree program of the Institute, has been examined by the thesis committee duly appointed by the Institute. The committee finds the work done by the candidate satisfactory and recommends that the report be accepted.



Dr. Harvinder Kaur
Jassal

Dr. Kamal P. Singh



Dr. Ananth Venkatesan
(Supervisor)

Dated: May 24, 2021

Declaration

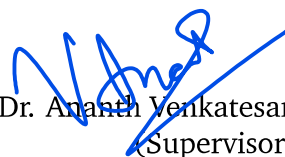
The work presented in this dissertation has been carried out by me under the guidance of Dr. Ananth Venkatesan at the Indian Institute of Science Education and Research Mohali. This work has not been submitted in part or in full for a degree, a diploma, or a fellowship to any other university or institute. Whenever contributions of others are involved, every effort is made to indicate this clearly, with due acknowledgement of collaborative research and discussions. This thesis is a bonafide record of original work done by me and all sources listed within have been detailed in the bibliography.



Sonell Malik
(Candidate)

Dated: May 24, 2021

In my capacity as the supervisor of the candidate's project work, I certify that the above statements by the candidate are true to the best of my knowledge.



Dr. Ananth Venkatesan
(Supervisor)

Acknowledgements

I would like to thank my guide Dr. Ananth Venkatesan for his brilliant guidance and the opportunity to work in his amazing lab. He not only guided me through experiments in the lab but also helped me in making decisions for future studies. I thank him for his patience and the countless discussions that guided me through experiments. He always has brilliant ideas and new approaches for every experiment and it inspired me a great deal to continue research in a related field. His support at every step has made this thesis possible.

I would also like to thank Shelender Kumar for helping out every time I faced difficulty in the lab. His simplified understanding helped me grasp a lot of topics and carry out experiments. I am very grateful for his immense contribution to this thesis. I thank lab seniors Dr. Radhikesh, Shyam Sunder and Pankaj for their guidance and helpful discussions every time I needed help or felt lost about theory or experiment. They were always available to guide through the experiment or to discuss theory and future directions in the experiments. In addition to this, I am very grateful to all lab members, seniors and colleagues, for the great lab environment. It was fun to work in the positive inspiring atmosphere in the lab everyday. Light hearted discussions ranging all topics and everyone's friendly nature made this one year and previous experience in Ultra Low Temperature Lab a great experience which I am thankful for. I also want to thank my committee members Dr. H.K. Jassal and Dr. K.P. Singh for their valuable feedback.

I would like to thank Indian Institute of Science Education and Research Mohali for the brilliant environment conducive to research and better scientific temperament. The institute has helped me grow over the last five years and I am grateful to have been part of this prestigious institute. I would like to extend thanks to Dean of Academic Affairs and Dean of Student Affairs Office for helping out with administrative work. I would like to thank the physics department for the brilliant course work and brilliant teaching. I would also like to thank the Library for providing access to study resources both online and offline.

I would also like to thank my family Mr. Surjeet Malik, Mrs. Prem Malik and Mr. Prateek Malik for their never ending support and belief in me. They always encouraged me to pursue my dreams and supported me at every step. They inspire me to work hard everyday.

This thesis and these wonderful five years would not have been the same without my amazing friends who I am grateful for everyday. I was lucky to find guidance, support and fun company with them. I thank them for making me a better person and for inspiring me throughout.

List of Figures

1.1	A diagram showing cooper pair formation due to a mobile lattice displacement. Source [IPad18]	3
1.2	An SNSPD in meander geometry. Source [SSH ⁺ 17]	5
1.3	A schematic of energy transfer after photon absorption in an SNSPD. T_e is the electron temperature, T_ph is the lattice (phonon) temperature. $\tau_e - ph$ is the electron-phonon coupling time constant and $\tau_ph - sub$ is the time constant for phonon-substrate coupling which occurs from phonon-phonon scattering. Source [Ban17]	6
1.4	Detection cycle of an SNSPD. τ_1 is the time taken for the current to decay across the nanowire and τ_2 is the time taken for the current to reach the same value as before. Source [NTH12]	7
1.5	An equivalent lumped circuit for an SNSPD. Source [NTH12]	7
2.1	The sputtering chamber from excel instruments in ULTP Lab. Source [Hug16c]	10
2.2	Diagram of sputtering setup. Source [Hug16c]	12
2.3	A picture of Sputtering chamber with confined plasma visible for dc magnetron sputtering on the left and rf magnetron sputtering on the right.	13
2.4	A sputtering gun from excel instruments. Source [Ins16]	14
2.5	Diagram of electron-beam evaporation setup. Source [Hug16b]	16
2.6	The electron-gun evaporation chamber from excel instruments in ULTP Lab.	16
2.7	Diagram of thermal evaporation setup. Source [Hug16d]	18
2.8	Thermal Evaporation chamber in ULTP lab.	18
3.1	Crucible used to hold e-beam target. Structures with many buckets can hold multiple targets which can be changed as the crucible are rotated.	23
3.2	A picture of Scanning Electron Microscope from JEOL in the cleanroom.	25
3.3	Transverse view of a MoGe thin film on a silicon substrate.	27
3.4	EDX spectrum. The y-axis represents the intensity of photons of different energies. The x-axis marks the energy of photons detected.	28
4.1	Circuit diagram for T_c measurement. The sample mounted on a PCB is mounted in a Dilution refrigerator where the temperature can drop down to 10 mK. The reflected signal is coupled to an input port of the lock-in via a directional coupler.	32

4.2	Quartz Crystal (with MoGe deposited on it) connected onto a PCB and loaded in dilution fridge.	32
4.3	The resulting graph for reflected voltage (volts) as a function of temperature (Kelvin). An increase in reflected signal is observed starting at 1K. This indicates transition to superconductivity. The input signal had a frequency 2.35 MHz.	33
4.4	PCB with a microstrip etched on it. A TiPd sample deposited on a silicon wafer is pasted on the microstrip line upside down. One end of the microstrip is grounded via a $50\ \Omega$ surface mount resistor and the other end connects with the input probe which also carries any reflected signal.	34
4.5	Reflected signal (in dBm) for microstrip in close contact with a superconductivity thin film measured at 2.35 MHz.	35
5.1	Circuit diagram for signal readout. The SNSPD is modeled as resistor and inductor in series. The bias tee values for capacitor and inductor are shown in the figure. The output pulse across the shunt resistor is amplified and recorded in an oscilloscope. Source [YHLWJ+15] . . .	43
5.2	Schematic showing vortices running from the top of a superconductor to the bottom with flux pinned due to a) weak pinning centers, b) line defects, c) crystal boundaries, d) large pinning centers like foreign atoms, lattice irregularities or nanoparticles. [OPR+12]	44
4	The thin film capacitor device. All the layers are shown here.	51
5	A PCB with sketched arms made for measuring resistance between the two plates of a thin film capacitor.	52
6	Thin film capacitor with top contact of gold wire attached via indium solder.	53
7	The setup used to measure resistance between the top and bottom plates of fabricated capacitors. Keithley 2000 multimeter is used as the ammeter, Agilent UB001A DC power supply is used to create a voltage between the two plates of capacitor.	53
9	The circuit of a capacitance bridge used to measuring capacitance. Source [Ste06]	56

List of Tables

3.1	MoGe thin film EDX result of atomic ratios when dc current supplied to Molybdenum target is 0.16A.	29
3.2	MoGe thin film EDX result of atomic ratios when dc current supplied to Molybdenum target is 0.17A.	29
3.3	MoGe thin film EDX result of atomic ratios when dc current supplied to Molybdenum target is 0.18A.	29
3.4	TiPd thin film EDX result of atomic ratios.	30
3.5	Final thin film results.	30

Abbreviations

EDX Energy-dispersive X-ray spectroscopy [i](#), [iii](#), [vii](#), [ix](#), [22](#), [25](#), [27-30](#), [34](#)

PCB Printed Circuit Board [i](#), [ii](#), [1](#), [31](#), [32](#), [34](#), [35](#), [51](#), [52](#), [54](#)

QCM Quartz Crystal Microbalance [18](#), [19](#), [51](#)

SEM Scanning Electron Microscope [i](#), [vii](#), [ix](#), [25-27](#), [42](#)

SNSPD Superconducting Nanowire Single Photon Detector [i](#), [ii](#), [vii-ix](#), [3-7](#), [21](#), [41-44](#)

SPAD Single Photon Avalanche Photodiode [4](#)

Contents

List of Figures	i
List of Tables	iii
Contents	vii
1 Introduction	1
1.1 Thin Films	1
1.2 Superconductivity	2
1.2.1 Superconductivity in MoGe	3
1.2.2 Superconductivity in TiPd	4
1.3 Superconducting Nanowire Single Photon Detector (SNSPD)	4
2 Experimental Techniques	9
2.1 Sputtering	9
2.1.1 Plasma formation and DC Sputtering	10
2.1.2 RF Sputtering	12
2.1.3 Experimental working	13
2.2 Electron-Beam Evaporation	15
2.2.1 Experimental working	16
2.3 Thermal Evaporation	17
3 Fabrication of Thin Superconducting Films	21
3.1 Depositing Molybdenum-Germanium thin films	21
3.2 Depositing Titanium-Palladium thin films	22
3.3 Annealing the TiPd samples	24
3.4 Thickness measurement and EDX	25
3.4.1 Imaging on SEM	25
3.4.2 Energy-dispersive X-ray (EDX) spectroscopy	27
4 Measurements	31
4.1 Quartz Crystal Method	31
4.2 Microstrip method	34
4.3 Theory	35
4.3.1 Theory of Diamagnetism in Superconductors	36
4.3.2 Transmission Line and Magnetic Coupling	38
4.4 Comparing the two methods	40

5	Review and Future Work	41
5.1	Superconducting Nanowire Single Photon Detector (SNSPD): Experimental guide	41
5.2	Vortex pinning experiments	43
	Bibliography	45
	Appendix A: Growth of Capacitor for Magnetocapacitance Studies	49
A.1	Fabrication of Nickel thin film capacitors	49
A.1.1	Pre-treatment	49
A.1.2	Depositing Nickel	50
A.2	Making the PCB and contacts	51
A.3	Challenges	53
A.4	Steps to overcome the challenges	54
A.5	DC measurement	55
A.6	Capacitance measurement	56

Abstract

Superconducting thin films are an active area of research for their applications in device fabrication like 2D circuits, 2 dimensional electron gas system, and research in 2D properties like quantum hall effect, spin currents etc. Thin film fabrication methods are instrumental in making devices like Josephson junction (trilayer devices), superconducting nanowire single photon detector, Superconducting Quantum Interference Devices, etc. The thesis discusses four methods of thin film deposition which were used to deposit molybdenum, germanium, titanium, palladium and nickel. These methods have been used for depositing a variety of other materials and the process and theory behind each method will act as a guide for selection of a suitable method for each material to be deposited. [Chapter 2]

The thesis goes on to describe superconductivity in Molybdenum-Germanium alloys and Titanium-Palladium alloys, and other properties suitable especially for SNSPD device and for studying vortex motion in type II superconductors [Section 1.2]. Their deposition methods and resulting atomic concentrations are detailed in chapter 3 of the thesis along with an experimental and theoretical guide to SEM imaging [subsection 3.4.1] and EDX measurements [subsection 3.4.2].

Chapter 4 in the thesis discusses one-probe transition temperature measurement using two methods both of which use Meissner effect and a qualitative analysis using condensed matter theory (London equation). For the microstrip method, the analysis is done in combination with telegrapher's equations. [Section 4.3]

The final chapter 5 discusses future work and experimental guide to fabricate and study Superconducting Nanowire Single Photon Detector (SNSPD) devices and for vortex motion studies using thin film devices. The aim of this chapter is to detail ideas that could not be implemented, which will hopefully be carried out in the future.

The appendix 5.2 of the thesis details extra work, fabricating thin film nickel capacitor which will help study magnetocapacitance effects. This section details fabrication methods, dc measurements and future work in this experiment.

Chapter 1

Introduction

1.1 Thin Films

A thin film is a layer of material deposited on a substrate with a thickness ranging from micrometers to nanometers. Thin films have been of great importance and they can be found in household items like mirrors, in laptops in the form of thin film batteries, on cameras and lenses for aberration correction, etc. They have also played a fundamental role in Printed Circuit Board (PCB)s development and the revolution that two-dimensional circuits brought about. Thin films have also helped study two-dimensional properties of materials, which in many cases are different from bulk properties, a significant example being quantum wells and 2-dimensional electron gas. In the GaAs-AlGaAs system, a thin layer of GaAs is sandwiched between layers of AlGaAs. The two materials have a mismatch of energy bands which leads to an almost 2-dimensional region at the interface of AlGaAs and GaAs where electrons find a lower energy state and collect. Quantum wells have been used to make photodetection in infrared imaging, high electron mobility transistors etc.

Hall effect and Quantum hall effect have been studied and are still examined for novel phenomena and these were possible due to the development of thin film technology. Many other devices can be made on thin films to study spintronics, superconducting properties etc. Above all, these devices are very small and can be fit on a chip as small as $1\text{ mm} \times 1\text{ mm}$. Their small size makes studying their properties at low temperatures easy because a dilution refrigerator has limited space. Therefore thin films are of great importance for technological and scientific development. In this thesis, different methods of thin film fabrication are explained and their applications are discussed.

1.2 Superconductivity

Superconductivity is the phenomenon in which resistance in a conductor vanishes to zero. This phenomenon, however, is different from perfect conductivity and the difference arises from the Meissner effect. In the presence of a changing magnetic field, currents are induced in a conductor to keep the net flux through it constant. Therefore, if a conductor is cooled to zero Kelvin in the presence of a magnetic field, the final flux through the conductor will be non-zero. Superconductors show a different response to this experiment. When a conductor is cooled, whether the initial flux is zero or not, the final flux is always zero when it becomes a superconductor. Meissner and Ochsenfeld discovered this phenomenon experimentally in 1933 and it soon came to be known as Meissner effect. Perfect diamagnetism arises from shielding currents on the superconductor's surface which cancel any magnetic field inside.

The shielding current that occurs spontaneously when a conductor becomes a superconductor requires energy; therefore, the superconducting state must have lower free energy below the transition temperature. The maximum amount of field a superconductor can expel, therefore, depends on the free energy gap between the conducting and superconducting states and this critical value of the field is called the thermodynamic critical field H_c , which depends on the temperature. Since a current carrying wire generates a magnetic field too, there is similarly a critical current density beyond which a superconductor loses its superconductivity.

Depending on the type of transition from normal to superconducting state in the presence of a magnetic field, superconductors have been categorised as type I and type II. Type I superconductors undergo an abrupt transition from superconducting to normal state when the magnetic field exceeds the critical value and the magnetic field penetrates the material. In type II superconductors, as the magnetic field increases, at the first critical magnetic field H_{c1} , tiny fluxoids (also called Abrikosov vortex or fluxon) appear in the superconductor, which allow magnetic field to pass through them while keeping the rest of the material superconducting. These fluxoids or vortices are a swirling current that allow magnetic field to pass through them. Each fluxoid allows a quantum of magnetic flux $h/2e$ to pass. As the magnetic field increases beyond H_{c1} , the number of fluxoids keeps increasing till the whole material becomes normal. The second critical field value that marks the complete transition to normal metal is written as H_{c2} . Type II superconductors have many applications, especially for making electromagnets that produce high magnetic fields. Superconducting wires made out of type II superconductors can withstand a high magnetic field due to a high H_{c2} value which has found applications in research and medical equipment such as MRI (Magnetic Resonance Imaging).

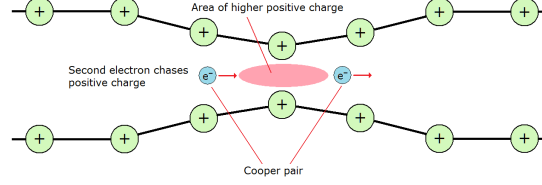


Figure 1.1: A diagram showing cooper pair formation due to a mobile lattice displacement. Source [Pad18]

The basic idea behind superconductivity is the pairing up of electrons which are called Cooper pairs below a certain transition temperature T_c . Electrons have half-integer spins and therefore follow Fermi statistics, but after pairing up, they have net zero spin and follow Bose statistics which allows all (Bosonic) pairs to occupy the zero energy level. The BCS theory (Bardeen–Cooper–Schrieffer theory) explains the pairing in terms of electron-phonon interaction. Phonons are quanta of lattice vibrations. As an electron moves through a region, it can polarize a part of the lattice creating a net positive charge in the region from which atoms have shifted which attracts another electron before the atoms have a chance to come back to the equilibrium position (see Fig 1.1).

1.2.1 Superconductivity in MoGe

Molybdenum and Germanium alloy films have been used to study Abrikosov vortex memory devices and other properties like localization and metal-insulator transition. [Kub88] Thin films of MoGe can be both amorphous and crystalline based on the thickness. Very thin films are usually amorphous which helps make devices like photon detectors. The coherence length of crystalline superconductors is much larger than amorphous ones, therefore, if a Cooper pair breaks down due to the absorption of a photon, the voltage generated in the wire due to the unpaired electrons will take more time to die out (i.e., the relaxation time will be more). Amorphous films have a shorter coherence length and a shorter relaxation time. In MoGe films, the main crystalline phase is A15 which is more stable than the amorphous phase at temperatures above 20 K for thickness greater than a few thousand microns. MoGe has been observed to have shown superconductivity only for germanium concentration in the range 10 % - 30%. Further reasons for choosing MoGe as our choice for SNSPD device fabrication have been discussed in section 5.1.

For Molybdenum and Germanium bulk alloy, the highest T_c has been reported to be around 6.8 K for $\text{Mo}_{0.75}\text{Ge}_{0.25}$. For thin films, the highest T_c is obtained for $\text{Mo}_{0.75}\text{Ge}_{0.25}$ in the range 4.5 K (7.5 nm film) to 5.5 K (50 nm film) depending on

the thickness of the film. [Kub88] [LKHX10] The thinner a film, the lower its T_c . It forms a type II superconductor. MoGe is deposited using sputtering because Germanium is a semiconductor. Semiconductors can be deposited in an energy efficient way using rf sputtering. The two materials can be co-deposited with Molybdenum deposited by dc sputtering and Germanium by rf sputtering or an alloy of the desired composition can be evaporated using rf sputtering.

1.2.2 Superconductivity in TiPd

Titanium becomes superconducting at 0.36 K and it has been studied extensively for the alloy superconductors that it forms with other elements. Titanium's alloys with Niobium, Hafnium and Zirconium and Palladium not only show a significantly higher T_c than Titanium metal, but also show superior mechanical properties, high critical field and current density making it suitable for use in microcircuits.

Titanium Palladium alloy has shown superconductivity and the highest T_c has been found for $\text{Ti}_{0.85}\text{Pd}_{0.15}$. This value is a local maxima and concentrations around this value show slightly lower T_c with $\text{Ti}_{0.8}\text{Pd}_{0.2}$ at 3.67 K and $\text{Ti}_{0.92}\text{Pd}_{0.08}$ at 3.65 K. TiPd forms a type II superconductor. $\text{Ti}_{0.85}\text{Pd}_{0.15}$ shows H_{c1} of 193 Oe and H_{c2} of 108.7 kOe. TiPd has a body centered cubic structure same as β -Ti phase. [RDMMPPE20]

1.3 Superconducting Nanowire Single Photon Detector (SNSPD)

Superconducting Nanowire Single Photon Detector have emerged as practical devices for photon detection in the infrared range. Superconductors have been used for photon detection in the form of kinetic inductance detector, transition edge sensor, and superconducting tunnel junction etc. SNSPDs have proven to be better than any of these devices because of faster recovery time and better detection efficiency and better timing precision. SNSPDs have better signal to noise ratio than their main competitor in the long wavelength detection regime, Single Photon Avalanche Photodiode (SPAD). Single photons detectors are instrumental for experiments like quantum key distribution, LIDAR, characterisation of quantum emitters, space-earth communication etc. They show superior photodetection rates for a wide range of wavelengths ranging from 200 nm to above 2 μm . SNSPDs have also shown promise in detecting the photons of wavelength around 1550 nm which is used for long distance communication via optic fibers due to minimum signal attenuation.



Figure 1.2: An SNSPD in meander geometry. Source [SSH⁺17]

These devices can be fabricated on a thin film of superconducting material. Usually, a meander geometry is created and the thin wires act as photon detection points (Fig 1.2). A single photon detector works by creating an electrical pulse upon absorption of a photon. This signal must be distinguishable from the background noise.

When a superconductor absorbs photons, the equilibrium state is disturbed and the energy of the photons breaks some Cooper pairs, which form excited quasiparticles (or hot electrons), leading to a finite resistance. The resistive region in the superconductor where quasiparticles form is called a hotspot. These quasiparticles are at a higher temperature than the Cooper pairs. The quasiparticles lose some energy via inelastic scattering resulting from electron-electron and electron-phonon interactions. The quasiparticles gradually recombine when their energy decreases and the energy transferred to the phonons in the lattice is transferred to the substrate, which acts as a heat sink (Fig 1.3). Qualitative treatment of the system predicts that the size of a hotspot made from absorbing an infrared photon will be less than a hundred nanometers which should be comparable to the width of the nanowire in an SNSPD. A photon can disrupt hundreds of Cooper pairs forming a hotspot. [YKD⁺07]

The nanowire is kept well below its transition temperature and a current just below the critical current is directed along the nanowire. The hotspot formed in the region might not be wide enough to cover the entire width of the nanowire, but it forces the supercurrent to go around that region, which increases the current density in the adjacent parts of the nanowire. Since the current density

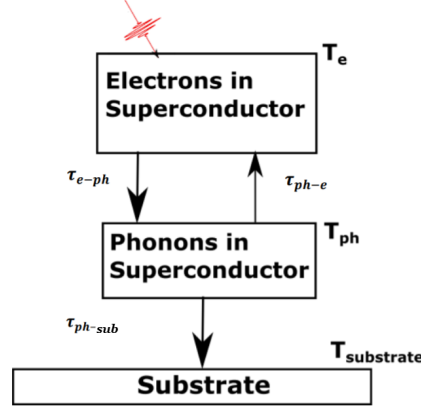


Figure 1.3: A schematic of energy transfer after photon absorption in an SNSPD. T_e is the electron temperature, T_{ph} is the lattice (phonon) temperature. τ_{e-ph} is the electron-phonon coupling time constant and τ_{ph-sub} is the time constant for phonon-substrate coupling which occurs from phonon-phonon scattering. Source [Ban17]

was already very close to the critical current density, the surrounding regions also lose superconductivity till the whole width becomes resistive. The region now acts like a resistor with time varying resistance, and a finite voltage pulse is generated until the region reaches equilibrium again. This pulse is detected by a circuit connected to the nanowire, thus indicating photon detection. This process of photodetection is explained in Fig 1.4.

The resistive part of SNSPD can be modelled as a time varying resistor ($R_n(t)$) and the kinetic inductance (L_k) of the rest of the superconducting wire is modelled as an inductor. When the nanowire forms a resistive barrier, the current is redirected to the shunt circuit via Z_0 as seen in Fig 1.5, where Z_0 is less than the resistance in the nanowire (in normal state). The current across the nanowire starts to decay as soon as the photon is absorbed and it quickly reaches zero in a duration $\tau_1 = L_k / (Z_0 + R_n(t))$. Reduction of current across the wire reduces Joules heating and the hotspot starts to cool down. The time taken for the hotspot to disappear and supercurrent to come back to normal is $\tau_2 = L_k / Z_0$ which is much larger than τ_1 . The SNSPD does not detect a photon for a duration $\tau = \tau_1 + \tau_2 \simeq \tau_2$ which is known as the dead time. Dead time can be reduced by reducing τ_2 which is inversely proportional to L_k that is by reducing the nanowire's total length or by increasing its width.

Large area meander geometry SNSPDs have good actual detection efficiency. A larger meander length leads to longer jitter time and longer dead time. Ultrathin nanowires show better registering efficiency. The meander geometry is

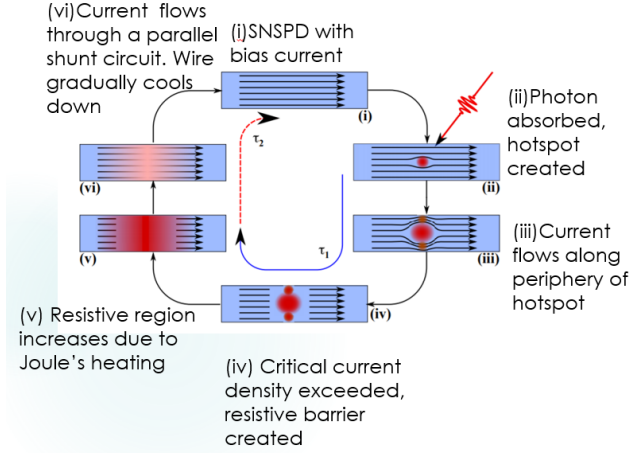


Figure 1.4: Detection cycle of an SNSPD. τ_1 is the time taken for the current to decay across the nanowire and τ_2 is the time taken for the current to reach the same value as before. Source [NTH12]

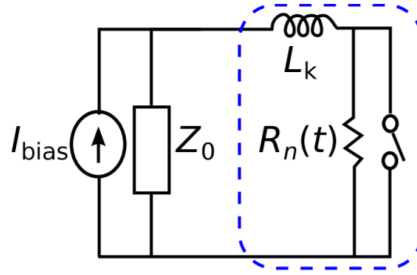


Figure 1.5: An equivalent lumped circuit for an SNSPD. Source [NTH12]

characterised by filling factor which is the ratio of nanowire surface to total substrate surface. A higher filling factor shows better detection efficiency but with increasing filling factor, the fabrication becomes trickier. These intricate devices are fabricated using electron beam lithography. The nanowires must have a uniform width throughout their length to obtain high detection efficiency. The width of the wires can be fine tuned for detecting photons of different wavelengths.

Chapter 2

Experimental Techniques

Thin film fabrication can be done by using physical or chemical methods. Most thin film deposition methods are chosen based on the properties of the material we want to deposit and the thickness of the film. Methods like molecular beam epitaxy and atomic deposition layer can give us accuracy up to a single layer of atoms or molecules. Other methods like spin coating, dip coating give a much thicker layer and control on the thickness of the order of a few microns at best.

The materials to be deposited also govern the method chosen for deposition. Metals with a low enough melting point can be deposited by using thermal evaporation. Materials requiring higher temperatures are evaporated using sputtering or electron gun evaporation which heat the target selectively. The latter methods can also be used to deposit semiconductors like silicon and germanium. A third limiting factor is the cost involved. Materials like gold and palladium are costly; therefore, obtaining a target for e-beam evaporation will be very expensive. They are therefore deposited using thermal evaporation and sputtering, respectively.

The following chapter will discuss three methods of thin film deposition: Sputtering, electron beam evaporation, and thermal evaporation. These are the methods employed to deposit the films that are later studied in this thesis.

2.1 Sputtering

Sputtering is a physical vapor deposition method for thin films. Atoms are ejected due to the bombardment of high-energy ions on the target. The gas used is usually inert, like Argon for higher atomic weight targets and neon for targets of lower atomic weight for efficient momentum transfer. The gases can also have some proportion of reactive gases to get compound thin films like oxides and nitrides. The atoms ejected from the target are deposited on a substrate

which is placed in close proximity and in the direction that the ejected particles travel. Sputtering is of many types depending on the properties of the target, namely dc sputtering, rf sputtering, magnetron sputtering, ion beam sputtering, reactive gas sputtering etc. The sputtering chamber shown in the figure can do both dc and rf sputtering (Fig 2.1). These techniques are discussed in the following sections.

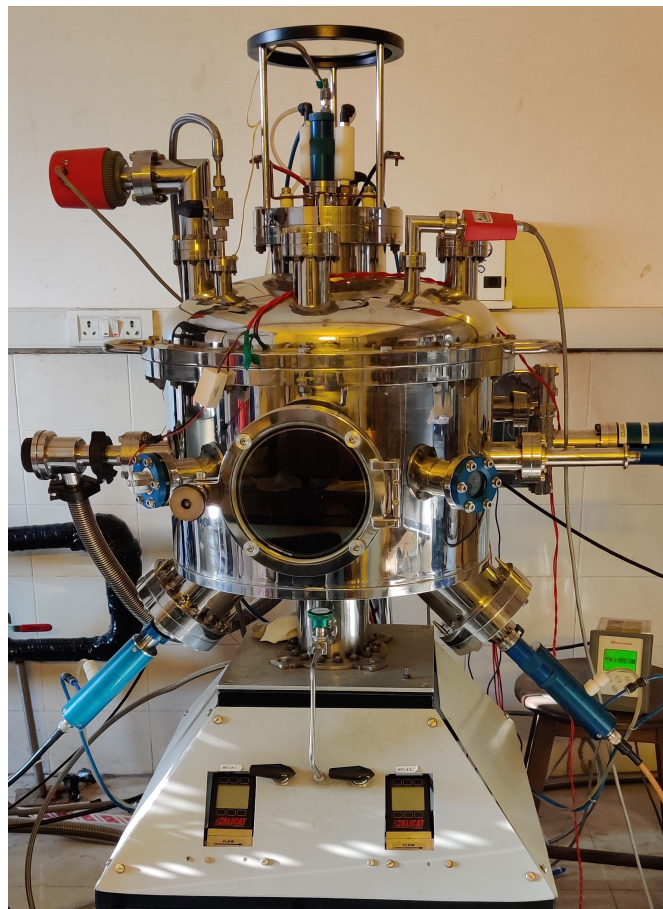


Figure 2.1: The sputtering chamber from excel instruments in ULTP Lab. Source [Hug16c]

2.1.1 Plasma formation and DC Sputtering

The sputtering chamber is initially put in high vacuum (of the order of 10^{-7} Torr) to remove reactive gases and water vapor. Argon gas is then filled into the chamber until an optimal pressure is achieved so as to create and maintain

plasma. Initially, one or two stray electrons present near the cathode are accelerated as they move towards the anode and they strike any Argon atoms they meet on the way. A collision ionizes the atom, thus releasing another electron which strikes other atoms, thus creating a cascade and ionizing most of the gas leading to a breakdown. The breakdown depends on the voltage applied between the anode and the cathode and the distance between them. If the pressure of the gas is too low, plasma won't form since there won't be enough collisions to form a cascade. If the pressure is too high, a free electron won't accelerate enough to ionize the Argon atom it hits, and there won't be any plasma. Therefore, the Argon gas pressure must be just right to achieve breakdown and create a plasma that will be self-sustaining. The gas pressure must therefore, range from 10^{-2} to 1 Torr, and the plasma density ranges from 10^{10} to 10^{12} per cm^3 when the voltage maintained between the anode and cathode remains constant, while the current slowly increases as breakdown approaches. Once the plasma is created, it is visible due to multiple electron recombination events which produce light, giving it a distinct glow. The glow is visible close to the cathode where the electrons have lower energies. Closer to the anode, electrons are far too energetic to recombine. Sputtering can be done once current is uniform across the whole target (cathode). This is called the abnormal discharge regime and it is achieved when the input power is high enough. [luce03]

When high energy ions hit the target, they can be reflected, adsorbed, sputter target atoms or even lead to electron and photon emission. Sputtering happens when the energy of the ions after accelerating across the electric field is between 10 eV and 10 keV because this range of energies is much larger than the atom's lattice binding energy and collisions can almost be considered elastic, leading to efficient momentum transfer. In addition to this, if the ion has mass comparable to the target atom, this also helps in momentum transfer and the target atom is ejected when a high energy ion strikes it. At lower energies (up to 50 eV) in the sputtering range, a single collision (oblique to allow the atom to escape the surface) can transfer enough momentum to overcome the lattice binding forces. When the energy of the incoming ions is higher, the ion transfers energy to an atom which goes off and strikes other atoms. This leads to energy being spread across the whole target and creating a cascade and multiple atom emissions. Sputtered atoms tend to have higher energies than thermally evaporated atoms.

Direct Current sputtering is one of the most basic and cost-effective methods for depositing conducting materials. A dc voltage in the range of 2-5 kV is applied between the anode and cathode. The ionized gas accelerates across the electric field between anode and cathode and leads to sputtering of the target material. The atoms that have been released reach the substrate and get deposited. These atoms have high energy and if they are bombarded with high energy electrons, they can be ejected from the substrate which will slow down

deposition. To avoid this, magnets are placed behind the cathode which traps electrons in the vicinity of the target. [Hug16a] This also leads to a higher current even when at lower pressures due to confinement of argon ions close to the cathode thus increasing sputtering yield.

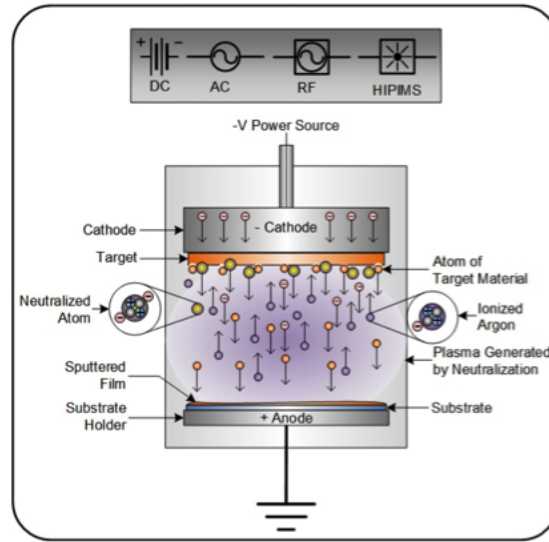


Figure 2.2: Diagram of sputtering setup. Source [Hug16c]

2.1.2 RF Sputtering

Targets that are not conducting, like semiconductors and insulators, will accumulate a charge if DC sputtering is used. This can lead to arcing and eventual die out of the sputtering process. Radio frequency sputtering is used to overcome this issue, which alternates the voltage applied across the target and substrate at radio frequencies, thus clearing up any charge buildup in each cycle. When the target acts as the cathode, ions from the plasma gas bombard the target leading to sputtering of the material. As the cycle progresses and the target becomes the anode, it attracts electrons which create a negative charge on the target which helps clear out the positive charge accumulated in the first half of the cycle. A charge accumulation can lead to discharge from the cathode into the plasma leading to non-uniform deposition, this is called arcing. RF sputtering leads to a more even erosion of the target thus increasing its longevity.

The presence of magnets behind the target material help to constraint electrons close by thus significantly reducing plasma discharge. This becomes even more important for rf sputtering since the alternating voltage does not allow enough charge build up to sustain a plasma without magnetic confinement. This

is called rf magnetron sputtering and it gives a high deposition yield even at low pressure. However, it must be noted that rf sputtering requires much higher applied voltage to achieve the same rate of deposition as dc sputtering. This leads to a further problem of overheating of the target material which can lead to target breaking. In addition, the rf circuit can overheat too.

2.1.3 Experimental working

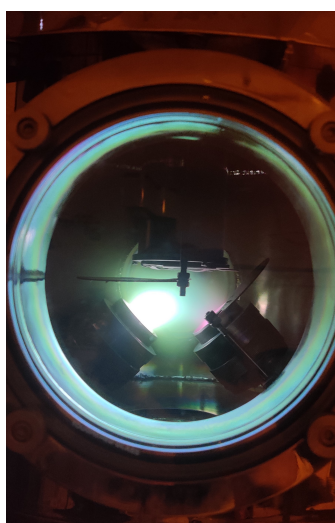


Figure 2.3: A picture of Sputtering chamber with confined plasma visible for dc magnetron sputtering on the left and rf magnetron sputtering on the right.

A vacuum of the order of 10^{-7} Torr was built in the chamber using a turbomolecular pump supported with a roughing pump. Following this, Argon gas was fed in at a rate of 30 sccm after putting the turbo pump in standby mode. The flow rate of Argon gas is controlled using a mass flow controller. The gate connecting the turbo to the chamber was adjusted to maintain the pressure around 5×10^{-2} Torr, the pressure at which deposition occurs. The deposition pressure fluctuates a little because of the running turbo pump which leads to a few variations in the dc voltage observed in both dc and rf sputtering.

DC Sputtering

The dc Sputtering, as mentioned above, works on an applied dc voltage. This voltage is applied with the help of an ADL dc power supply which can be operated in three modes: Current mode (in which the rate of current between anode

and cathode is kept constant); Voltage mode (in which the voltage between the anode and cathode is kept constant); and Power mode (in which the power is kept constant while current and voltage vary). The deposition of molybdenum was done using dc sputtering. Although a constant power mode is preferred for uniform deposition, the uniform current mode was chosen for two reasons, because it was in agreement with the recipe used by Banerjee et al. [BBD⁺17] used to create superconducting MoSi thin films and, because the dc gun would sometimes not create the plasma in power mode. In the dc supply, a current of 0.17 A was chosen since it gave the desired atomic concentration. In the constant current mode, this leads to a voltage ranging from 245-255 V and power ranging from 40 - 45 W in most depositions.

The sputtering chamber is connected to a sputtering gun, as shown in figure 2.4. The thick steel rod running in the center of the gun carries circulating cold water to prevent overheating of the target. The gun is attached to the dc power supply using a coaxial cable. The head of the gun contains the target and serves as the anode. A shutter can be seen at the bottom right end of the picture which can be opened and closed from outside the chamber to precisely control the duration of deposition. This entire setup forms the dc sputtering system used for depositing molybdenum.

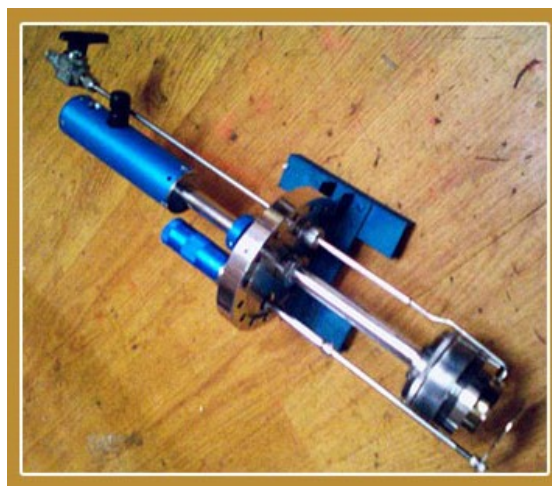


Figure 2.4: A sputtering gun from excel instruments. Source [Ins16]

RF Sputtering

The rf sputtering system contains a gun similar to that used for dc sputtering. In this case, the gun is connected to Seren R601 Radio Frequency Power Supply which can be set in the power mode via Seren MC2 Automatic Matching Network

Controller. The matching network controller is used for automatic impedance matching to transfer maximum power through the coaxial cable connected to the sputtering gun. The tune was usually at 49% and the load was at 75% with a dc voltage between the two cables in the coax ranging between 205 V and 220 V for all samples deposited. In the power mode, a power of 40 W was supplied to the germanium target.

2.2 Electron-Beam Evaporation

Also known as electron-gun evaporation, this method uses a beam of high energy electrons to evaporate the target material which then deposits on a substrate placed above the target. The material to be deposited is placed in a bucket shaped container called a crucible. A tungsten wire is used as a source of electrons which is directed at the target material using a magnetic field. A high voltage is applied across the tungsten wire to reduce its work function. A strong electric field at the emission point follows, which extracts electrons from the wire. The electrons accelerate in the electric field and are directed to the target material via a magnetic field. This stream of high energy electrons strikes the target and lose their kinetic energy very quickly, most of which becomes thermal energy (less than 10% of the kinetic energy is dissipated in the form of secondary electron emissions or X-ray emissions). This leads to evaporation of the target material in the region that the electron beam strikes and the evaporated atoms get deposited around the chamber including on the substrate. A diagram of the setup can be seen in [2.5](#). To ensure that the target material is used evenly, in most setups, a sweep is used which constantly sweeps the electron stream over the whole target material which avoids creating a hole in the target.

E-gun evaporation gives higher rates of deposition than sputtering and thermal evaporation thus leading to more dense films which also stick to the substrate better. Deposition rates as low as 1 nm/sec are also possible with e-gun evaporation. Charge accumulation can (and will most likely) occur when this method is used therefore, after opening the chamber, all metal surfaces and especially the tungsten wire and targets must be grounded to avoid getting a shock. This method is suitable to deposit materials with high melting points due to the localised and effective heating achievable in the process. This method also avoids impurities from the crucible since only the target heats up and not the crucible. The high voltage applied and the high heating rate from e-beam lead to a requirement of cooling which is usually accomplished by running cold water in close contact with components that heat up. It is also important to note that magnetic metals should not be deposited using e-gun because it would significantly affect, if not permanently alter, the working of the electron gun,

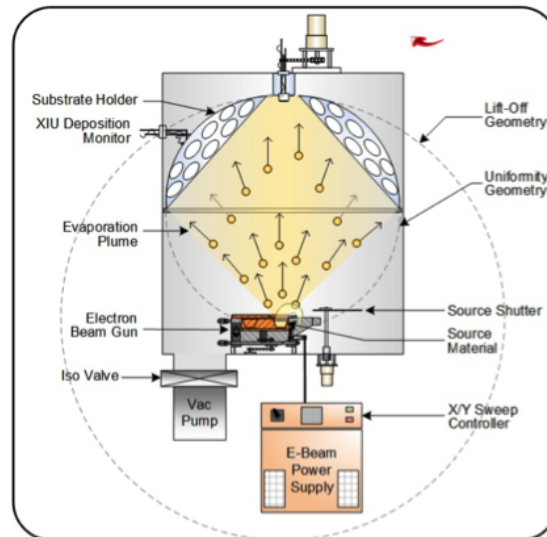


Figure 2.5: Diagram of electron-beam evaporation setup. Source [\[Hug16b\]](#)

making it harder to focus on the target.

2.2.1 Experimental working

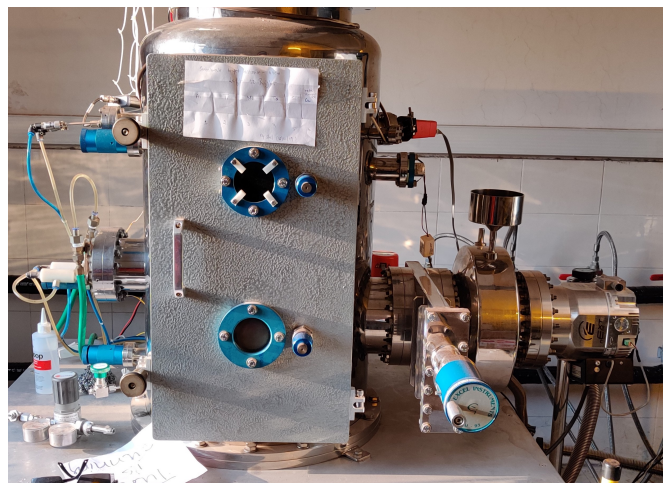


Figure 2.6: The electron-gun evaporation chamber from excel instruments in ULTP Lab.

The chamber is kept in a vacuum with pressure of the order of 10^{-6} Torr. A high voltage supply from Telemark is used to generate high voltage of up to

10 kV which is used for electron emission from the electron gun. This voltage is applied across the tungsten filament which acts as the electron source. This reduces the work function of the filament thus leading to electron extraction which is guided by the magnetic field onto the target. The Telemark TT controller can control all these parameters. The voltage across filament is set at 7.73 kV. Then, there is a 10 minute waiting time till the filament current reaches around 13 A. After this, the Cheetah Programmable Sweep must be switched on. This ensures even utilization of the target. Only after the filament current reduces and the sweep is turned on, the control can be flipped to emission current mode. It should be ensured that initially the switch is in filament current mode. The emission current, that is the amount of current being emitted from the gun onto the target, can be set depending on the desired rate of deposition. For titanium deposition, to maintain a deposition rate of around 1 Å per sec, the emission current was set at 58 mA.

2.3 Thermal Evaporation

Thermal evaporation is one of the most common methods of depositing thin films. Inside a vacuum chamber, a boat is placed which holds the material to be deposited. The boat is usually made of tungsten or molybdenum due to their high melting points which reduces chances of them mixing with the material to be deposited. To heat the pellet of the material of choice, a high amount of current is passed through the boat which heats up due to Joules heating. The pellet too gets heated due to conduction of the heat and starts to melt and evaporate. This method of deposition is susceptible to flash evaporation when most of the material evaporates off quickly and the thickness cannot be monitored accurately. The substrate is placed inverted right above the boat containing the pellet.

Constant cooling of the circuits involved is required due to high amounts of current passed which can go up to 200 A. As with all the other processes, but even more so here, a good vacuum is very important for thermal evaporation in order to achieve decent rates of deposition. This method however is least likely to damage the substrate in any way.

A high amount of current is passed using a power supply and currents up to 200 Amperes can be achieved, although such high values are not required for most materials. Once the boats are in place inside the chamber, the current is increased slowly so as not to put strain on the boat as it expands. The boat tends to get fragile when it is heated and any kind of pressure or too much weight from a lot of pellets can cause it to break. The substrate is placed on top of the boat to maximize the deposition rate. The rate of deposition can be monitored

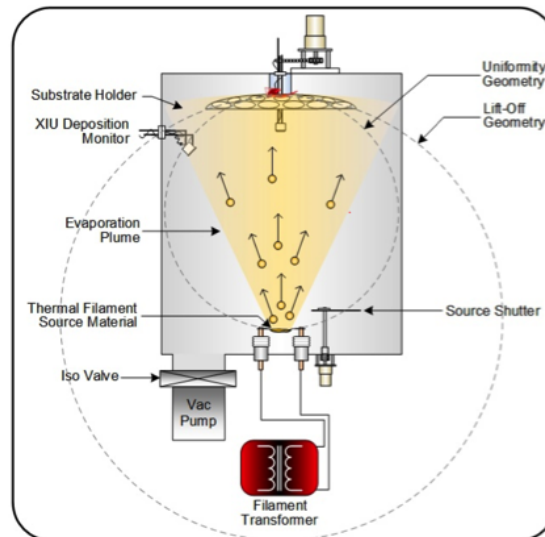


Figure 2.7: Diagram of thermal evaporation setup. Source [Hug16d]

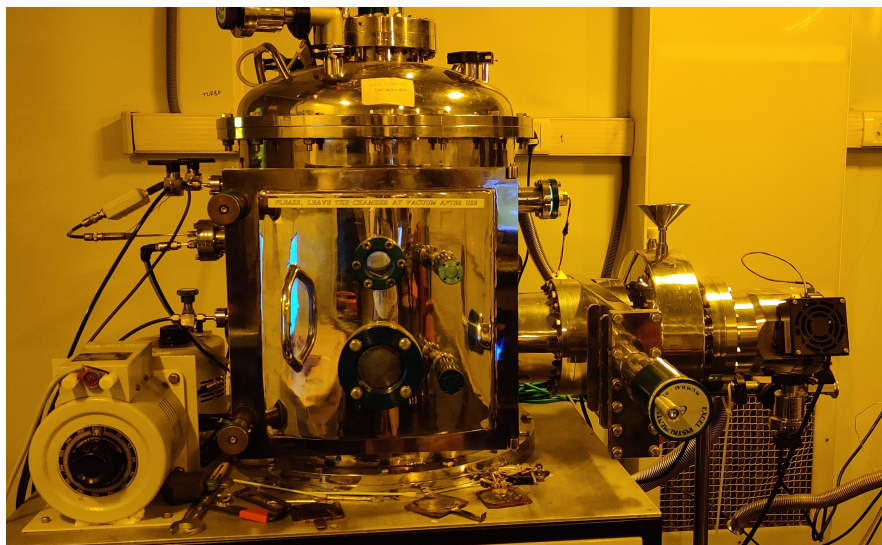


Figure 2.8: Thermal Evaporation chamber in ULTP lab.

using **Quartz Crystal Microbalance (QCM)** which can accurately determine the thickness of the film deposited if the tooling factor between the position of the **QCM** and boat is known. A roughing pump creates a rough vacuum of the order of 10^{-2} Torr while the turbo pump with the roughing pump in backing can improve the vacuum up to 10^{-6} Torr in this setup. The setup shown here has three stages on which boats can be placed so that three different materials can

be deposited or if one boat breaks deposition using another stage can continue, without breaking the vacuum. However, the boats can only be used one at a time. The tooling factor for the QCM must be changed for each boat accordingly.

For palladium deposition, a molybdenum boat was used. The current had to be maintained between 180 - 190 A to achieve a deposition rate of around 0.6 Å per sec. The current must be increased slowly to avoid flash evaporation which will lead to all of the palladium evaporating before it can be deposited.

Chapter 3

Fabrication of Thin Superconducting Films

Superconducting thin films can be used to make many devices like **SNSPDs**, SQUIDs, HEMTs etc. which have been of great interest to researchers and industry for applications in nanotechnology. Type II superconductors are also used for experiments in vortex pinning which can be used to increase critical current and critical field for superconductors. Electromagnets made of superconducting wires need a high critical current and critical field to achieve a high magnetic field. The thesis focused on fabrication Molybdenum-Germanium (MoGe) and Titanium-Palladium (TiPd) thin films which form type II superconductors.

3.1 Depositing Molybdenum-Germanium thin films

The desired thin films of MoGe were achieved by co-deposition of molybdenum and germanium in the sputtering chamber. The substrate used is a silicon wafer. The chamber was put in a vacuum, and the pressure should ideally be lower than 5×10^{-6} Torr to ensure a low enough concentration of oxygen and water vapors that allows the thin films to be superconducting. The aim was to achieve films of MoGe alloy in the concentration 70:30 which gives the highest possible T_c .

Molybdenum being a conductor, was deposited using DC sputtering while germanium was deposited using RF sputtering. The power and current applied at the targets were carefully selected based on the specification of the targets given by the manufacturer Kurt J. Lesker Company so as not to exceed the maximum power per unit area. The targets tend to break if the power supplied to the target is too high. A limitation in fast heat dissipation and thermal expansion can lead to breakage of the target and non-uniform deposition. After a plasma

is created in the chamber, the shutters must be opened after at least 5 minutes to give the plasma time to stabilize and get as uniform a deposition as possible. Multiple films were deposited with tweaks in power and current supplied to the targets and also the pressure of Argon during deposition. Through multiple trials and EDX examination (Section 3.4.2), the process to achieve specified compositions was perfected. The next step was to measure the thin films for superconducting transition temperature. A basic measurement of the samples was made in the dilution refrigerator in ULTP lab using a one probe measurement which will be described later.

Challenges

The DC gun in the sputtering chamber was shorting time and again and it required some disassembly and tweaks to get it running again. Another issue was with the shutter attracting the evaporated ions of germanium when it was opened but not kept far enough from the line of deposition. This led to non-uniform deposition across the substrate. These issues were identified and accordingly dealt with.

3.2 Depositing Titanium-Palladium thin films

Titanium was deposited using electron gun evaporation. It can also be deposited using thermal evaporation, but the thermal system here had been used to deposit Nickel and other ferromagnetic substances which are known to kill superconductivity if added to a sample, even in a tiny concentration. The substrate used is a silicon wafer. The aim was to achieve a concentration of 85:15 for Ti:Pd. Palladium was deposited in the same chamber using thermal evaporation. The thickness can be monitored as the metals are being deposited using quartz crystal microbalance. Since in the e-gun chamber, e-gun evaporation and thermal evaporation cannot be performed simultaneously, they were deposited one after the other. In all, four layers of titanium and palladium were alternately deposited to increase the mixing of the compounds and get an alloy of TiPd instead of a multilayered structure. The calculations for the thickness of each compound are as follows:

$$\frac{15}{85} = \frac{\rho_{Pd} \times x_{Pd}}{\rho_{Ti} \times x_{Ti}}$$

where ρ is the density of each element and x is the thickness. We want the film to have a thickness of around 80 nm. Therefore, assuming total thickness of titanium is 70 nm, we get

$$\frac{15}{85} = \frac{11.9 \times x_{Pd}}{4.5 \times 70}$$

giving us $x_{Pd} = 10.38nm$. Therefore, to deposit four layers of each element, each layer of titanium must be 17.5 nm and each layer of palladium must be 2.6 nm.

The e-gun chamber is put in a vacuum with pressure of the order of 10^{-6} Torr and the substrate is heated to 250°C before deposition to increase multilayer diffusion as the materials deposit. (The power supplied to the electron gun is selected based on the target). The titanium target is placed in a crucible (a bucket-like structure [Fig 3.1]) and an electron beam is directed at the target. The current of the beam is controlled based on the filament current supplied to the tungsten wire which ejects the beam of electrons. It must be ensured that the beam current is not too high to create a hole in the titanium target. This is prevented by using a beam rotation pattern that directs the beam in the shape of figure eight '8' and at the same time, rotates the beam at a high rate to get uniform evaporation from the titanium target.



Figure 3.1: Crucible used to hold e-beam target. Structures with many buckets can hold multiple targets which can be changed as the crucible are rotated.

Depositing palladium is a challenge because it has a high melting point and there is always a risk of flash evaporation with a pellet. Flash evaporation is a sudden high rate of evaporation which makes it difficult to control the thickness deposited and if the shutter is not opened in time, it could lead to all the palladium being evaporated before it can be deposited in the substrate. We should also not put more than two pellets on the boat because the boats are put under great stress when a high current is passed through them and they heat up. Having more than two pellets would increase the stress on the boat when it heats up. This might lead to the boat breaking before the evaporation or during the evaporation, thus creating a need to remove the vacuum and, to change the boat

before the deposition process can be continued. Therefore, current across the boat which holds the tungsten pellets must be increased very slowly (a good rough estimate is 10 minutes to get to 180A). The boat usually reaches palladium's evaporation temperature when the current across the boat is about 180A. The slower the current is increased, the lower this current value will get, but at the rate specified above, palladium starts to evaporate around 180A. It is also advisable to not increase the current beyond 190A even if the initial rate of deposition at 180A is very small because after 180A, the chances of flash evaporation increase significantly.

The shutters in the chamber must be opened once the rate of deposition is constant and around 1 Å per second.

3.3 Annealing the TiPd samples

To further help the diffusion of titanium and palladium layers, the samples were annealed i.e. heated in a continuous nitrogen supply. For this process, a Rapid Thermal Annealing Setup (RTA) was used. The setup consists of a tiny chamber in contact with a heater made of molybdenum. When high current is passed through the heater by connecting it to a voltage supplier (10 V), it heats up the chamber in which the samples are kept. The chamber is connected to a roughing pump to ensure there is no oxygen in the chamber and oxygen concentration is further reduced by creating a small but continuous supply of nitrogen across the chamber. The samples were annealed at two different temperatures 250°C and 450°C.

The chamber's temperature can be carefully controlled, including the rise time (i.e., the time required to reach the desired temperature) through the PID controller in the setup. PID stands for Proportional-Integral-Derivative and it works on a closed-control loop mechanism. The closed loop controls the variable temperature through a continuously modulated control. The proportional control works on the gross error in the control variable by continuously calculating the difference between the set value of the variable and the measured value called the gross error. The proportional controller corrects for the gross error in the control variable. There is a time lag associated with the error correction and from an integral of the gross error over time, the integral controller corrects for the residual error remaining after the proportional controller correction and increases rate of convergence to the set value. The above two processes together still do not solve the problem of overshooting. The differential controller works by calculating the previous rate of change of the gross error and makes the best estimate of error in the future and thereby controls the system in anticipation of the error about to occur.

We chose two temperature values to anneal different samples made in the same batch and decided to go ahead with the process that gave superconductivity in the desired range. The values chosen were considerably apart to show a difference in results (or so we expected) and they were well below the melting point of titanium, palladium and their alloy in our specific concentration. For annealing at 250°C, the rise time was chosen as 30 minutes which gives sufficient time for the PID controller to reach the set value in the chamber and stay stable. The power of heating is set at 70% of the maximum to avoid overshooting the set value. After the 30 minute rise time, the sample was annealed at a stable 250°C for 10 minutes, after which the system is left for cooling down to room temperature. The chamber takes 3-4 hours to cool down.

Initially, the connection between the voltage supplier and the heating element needed to be rewired and checked since the heater was not heating up, but the problem was soon figured out and resolved. Also, setting the value to 250°C in the PID controller resulted in a temperature less than 250°C at the end of 30 minutes. This required some trials and errors with different values of set point to get a stable 250°C at the end of the 30 minutes rise time and finally a value of 293°C gave a stable 251°C. This anomaly is possibly due to the nitrogen flow in the chamber which continuously carries out heat as it is pumped. These issues helped to gain a hands on experience on the instruments that used and to learn the skill of troubleshooting when something is not working.

3.4 Thickness measurement and EDX

3.4.1 Imaging on SEM

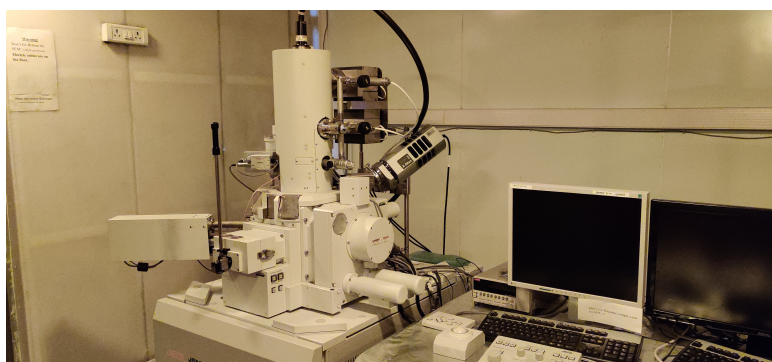


Figure 3.2: A picture of Scanning Electron Microscope from JEOL in the cleanroom.

The SEM can also be used for sample imaging. An optical microscope is

resolution limited due to wavelength of light. **SEM** uses high energy electrons for imaging. Electrons have a smaller wavelength (of the order of 1 nm) which can provide much better resolution. The **SEM** (Fig 3.2) [Ltd15] operated in the cleanroom here uses a field emission cathode in the electron gun to produce a narrow beam of electrons which are further accelerated in an electromagnetic field to reach high energies. The beam is further collimated using lenses and electromagnetic fields in the transverse direction.

The electron beam focused onto the sample produces a variety of signals from the electron beam-sample interaction, including backscattered electrons, secondary electrons, the characteristic X-rays [Sci21]. These signals are recorded in electron detectors. The secondary electrons arise from inelastic interactions with the sample and originate very close to the sample surface. The detector for secondary electrons is kept at an angle above the sample to increase detection efficiency. Secondary electrons are used to image the surface topography because they originate very close to the surface and the intensity of the detected electrons depends strongly on the angle of primary incident electron beam on the particular region on the sample surface. Backscattered electrons arise from the electrons in the primary beam, which penetrate a little deep (almost a micron) and get elastically scattered from the atoms in the sample and change trajectory. The degree of repulsion (shielding from valence electrons) and the number of backscattered electrons produced depends on the atomic number of the constituents. Therefore, atoms with large atomic number produce a stronger signal of backscattered electrons and produce a brighter image due to large number of signal electrons. The detector, in this case, is placed concentric to the primary electron beam with a hole in the middle. Interestingly, backscattered electrons can also give topographical information if electrons from individual quadrants of the detector are recorded and analysed.

SEM imaging can give a precise value of the thickness of deposited film for samples with thickness in the range of nanometers. This is required for samples made from sputtering, where due to unavailability of a quartz crystal microbalance, the thickness cannot be monitored as a sample is being deposited. Below are pictures from **SEM** imaging of MoGe deposited films Fig 3.3. The samples need to be cut in half after deposition because the deposition at the edges of the substrate will not be perpendicular; rather it will go around the edge with the thickness gradually decreasing. The angle too will not be close to 90° to the substrate, and it might give a misleading value of thickness. Instead, the sample should be cut right from the middle. Here, the deposition is even and the edge of the deposited film almost perpendicular to the substrate.

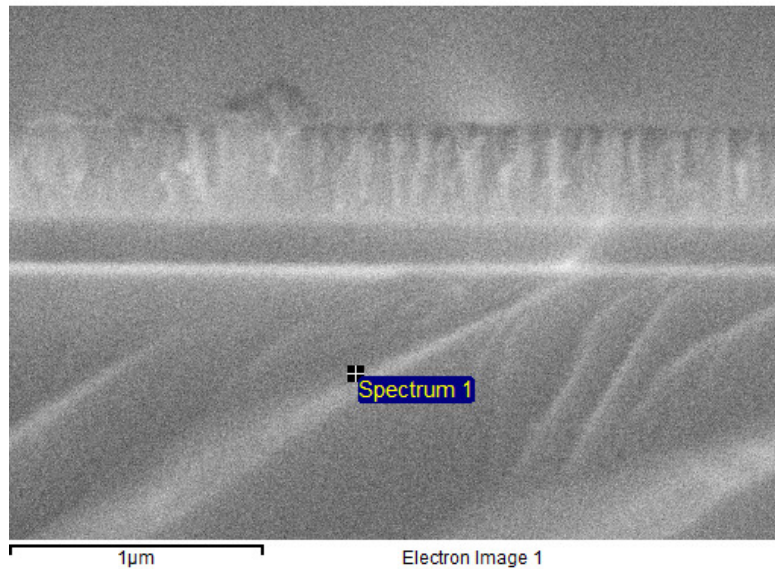


Figure 3.3: *Transverse view of a MoGe thin film on a silicon substrate.*

3.4.2 Energy-dispersive X-ray (EDX) spectroscopy

The Scanning Electron Microscope (SEM) was used for Energy-dispersive X-ray (EDX) spectroscopy which helps to determine the composition of the fabricated thin films. EDX works on the principle of a unique electromagnetic emission spectrum of each atom. In SEM, high-energy electrons are bombarded on the sample. The electrons penetrate the sample and as soon as they meet an electron orbiting an atom's nucleus, they share some of their energy with the electron resulting in the electron getting knocked off the orbital. This electron hole is filled in by an electron from an outer shell in the atom and results in the release of a photon corresponding to the energy gap of the two orbitals. The photon released when the electron is replaced, is detected in a spectrometer which records the energy and number of photons recorded for each energy value. The output of the spectrometer shows the peaks characteristic to each element constituent in the sample and the height of the peaks is proportional to their concentration. The set of peaks obtained for different transitions is unique to every element, thus helping us determine the elements in the sample in case that is unknown

and their respective percentage concentration too.

EDX was used to analyse all fabricated MoGe and TiPd thin film samples. For MoGe, different values of current to control the rate of sputtering of molybdenum were used. The resulting values for MoGe are give in tables 3.1, 3.2 and 3.3, and for TiPd in table 3.5. A spectrum for EDX measurement is shown in figure 3.4. The yellow peaks show energies of different photons absorbed. The system can auto-detect the constituents and in some cases, we can select them if they are known. The peaks are assigned to the elements based on the energies detected and characteristic energies of orbital recombination of electrons for each element. The height of the peak (y-axis) represents the intensity of photons of different energies. The x-axis marks the energy. The electron acceleration voltage was kept at 20 keV.

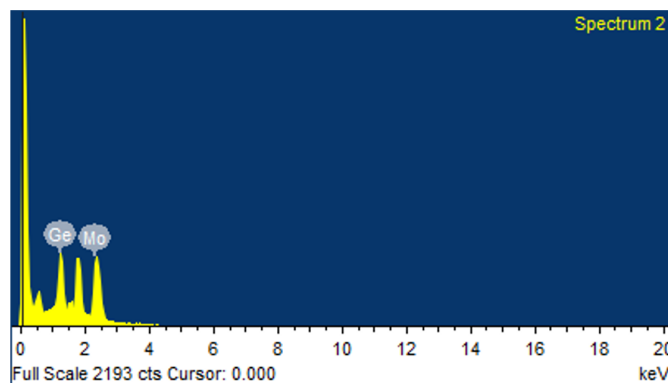


Figure 3.4: EDX spectrum. The y-axis represents the intensity of photons of different energies. The x-axis marks the energy of photons detected.

MoGe (at 0.16A to Mo)	
Molybdenum atomic percent- age	Germanium atomic percent- age
71.85	28.15
68.92	31.08
69.79	30.21
67.13	32.87
62.66	37.34
72.45	27.55

Table 3.1: MoGe thin film EDX result of atomic ratios when dc current supplied to Molybdenum target is 0.16A.

MoGe (at 0.17A to Mo)	
Molybdenum atomic percent- age	Germanium atomic percent- age
73.21	26.79
72.68	27.32
73.79	26.21
73.94	26.06
72.40	27.60

Table 3.2: MoGe thin film EDX result of atomic ratios when dc current supplied to Molybdenum target is 0.17A.

MoGe (at 0.18A to Mo)	
Molybdenum atomic percent- age	Germanium atomic percent- age
85.22	14.78
84.52	15.48
84.28	15.72
81.21	18.79
82.95	17.05
82.67	17.33

Table 3.3: MoGe thin film EDX result of atomic ratios when dc current supplied to Molybdenum target is 0.18A.

TiPd	
Titanium atomic percentage	Palladium atomic percent- age
80.59	19.41
79.26	20.74
85.91	14.09
78.80	21.20
79.76	20.24
76.03	23.97
82.17	17.83

Table 3.4: *TiPd thin film* EDX *result of atomic ratios.*

Final Results	
Mo:Ge	68.8 : 31.2 (0.16A to Mo)
	73.2 : 26.8 (0.17A to Mo)
	83.5 : 16.5 (0.18A to Mo)
Ti:Pd	80.4 : 19.6

Table 3.5: *Final thin film results.*

Chapter 4

Measurements

We needed to find the superconducting transition temperature of the films made using sputtering and electron beam evaporation. The expected transition temperature for the films is mentioned in Chapter 1. The transition temperature and even obtaining superconductivity depends greatly on the conditions of deposition. If there is a significant level of oxygen in the chamber during deposition, which can occur if the vacuum pressure obtained is higher than 10^{-5} Torr, the components of the film will have a high probability of oxidising. The oxides of the alloys used to make thin films not known to be superconducting, therefore, extreme care must be taken while fabricating. In addition to this, multiple other factors like pressure of argon during sputtering and substrate temperature during deposition in e-gun evaporation can play a pivotal role in deciding the superconducting transition temperature and even in determining if the films will be superconducting in the first place.

4.1 Quartz Crystal Method

The measurement aimed to use Meissner effect in superconductors to find the superconducting transition temperature T_C . The benefit of this method over other conventional four probe methods is the use of only one probe which saves space in the dilution fridge. In order to use the crystal, first, MoGe was deposited on a gold electrode Quartz crystal via sputtering. This crystal was then mounted on a PCB as shown in Fig 4.2. The crystal was held in place via clips and the clips were soldered onto the PCB. One electrode of the crystal is connected to the input probe from the lock-in and the other electrode is connected to the ground via a $50\ \Omega$ surface mount resistor. The resistor was connected to the PCB using silver paint.

The sample PCB is mounted in a dilution refrigerator with one wire con-

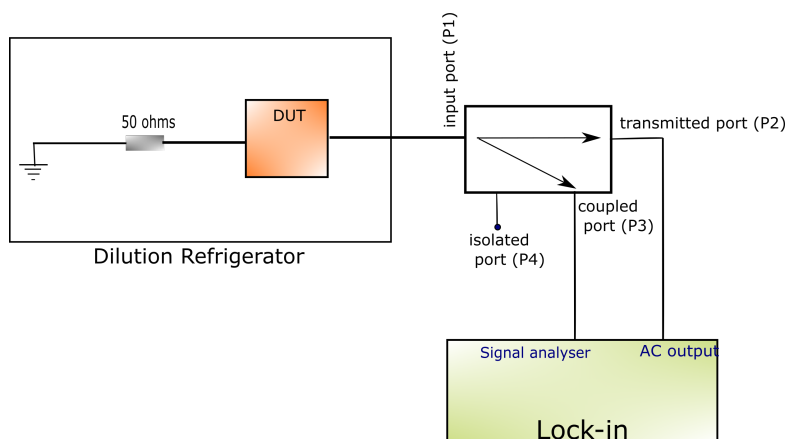


Figure 4.1: Circuit diagram for T_c measurement. The sample mounted on a **PCB** is mounted in a Dilution refrigerator where the temperature can drop down to 10 mK. The reflected signal is coupled to an input port of the lock-in via a directional coupler.

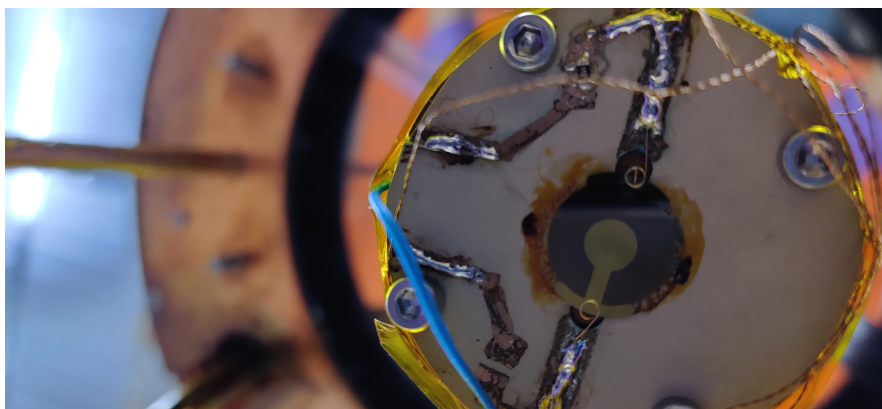


Figure 4.2: Quartz Crystal (with MoGe deposited on it) connected onto a **PCB** and loaded in dilution fridge.

nected to an electrode of the quartz crystal. The temperature in the refrigerator is gradually reduced and an AC signal is sent to the crystal via the input probe. The reflected signal (along the same wire) is recorded in the lock-in. The connection to the lock-in is shown in Fig 4.3. The wire connected to the quartz crystal is connected to a bidirectional coupler outside the dilution fridge (Figure 4.1). An AC signal is characterised by a continuous change in the magnitude and direction of the electric field which induces a magnetic field. Therefore, when the sample (thin film of MoGe deposited on the quartz crystal) becomes super-

conducting (below a certain temperature), it will expel most of the incoming AC signal leading to a sharp increase in the magnitude of the reflected signal.

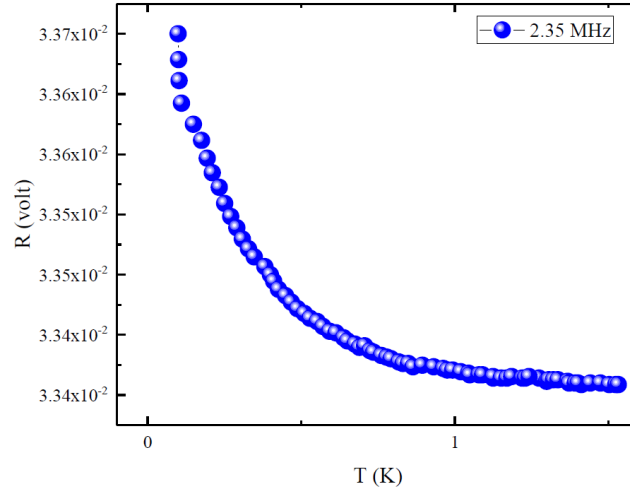


Figure 4.3: The resulting graph for reflected voltage (volts) as a function of temperature (Kelvin). An increase in reflected signal is observed starting at 1K. This indicates transition to superconductivity. The input signal had a frequency 2.35 MHz.

The reflected signal vs temperature is graphed in Figure 4.3. It shows an increase in reflected signal around 1 K which can be interpreted as a transition from normal state to superconducting state. We see an extended increase in reflected signal as temperature decreases. This can be attributed to Mattis-Bardeen theory of anomalous skin effect. When a high-frequency current is passed through a superconductor, it reflects most of the ac signal and a small amount of signal passes through travelling on the surface, within the penetration depth. At low temperatures, due to a decrease in skin depth to a value below the mean free path of normal electrons (in the two-fluid theory where both zero energy state paired electrons and excited electrons coexist in a superconductor), the surface resistance of a superconductor increases. As the temperature decreases, the skin depth will also reduce further increasing resistance, therefore, an increase in the reflected signal is observed with decreasing temperature. Shielding currents also counter the ac signal traveling on the surface of a superconductor to cancel any internal magnetic field. As far as the author knows, this is one of the first attempts to use a quartz crystal for one probe T_c measurement and a theoretical treatment is beyond the scope of this thesis. The T_c obtained from this experiment is much lower than the expected T_c for the MoGe film

in the specific concentration that was deposited. The **EDX** results showed that the concentration obtained was as expected which means that either there is some oxidation of the sample during deposition due to impure argon or the relative concentrations of the two components is spatially non-uniform and we don't have a good alloy mix.

4.2 Microstrip method

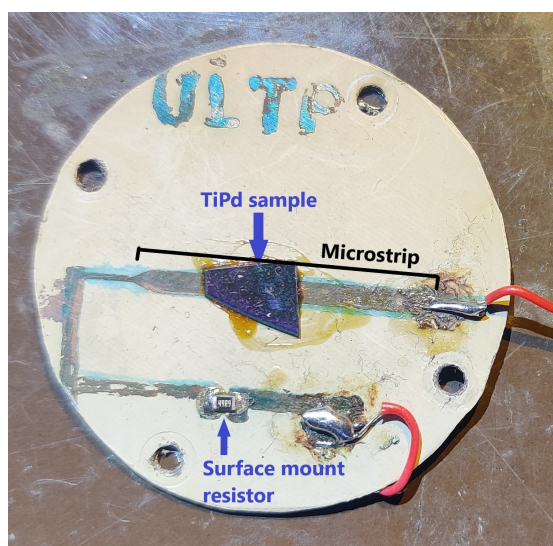


Figure 4.4: **PCB** with a microstrip etched on it. A TiPd sample deposited on a silicon wafer is pasted on the microstrip line upside down. One end of the microstrip is grounded via a $50\ \Omega$ surface mount resistor and the other end connects with the input probe which also carries any reflected signal.

A microstrip on a **PCB** can be used similar to the quartz crystal setup above (Fig 4.4). In this case, the superconducting material is placed in close contact with the microstrip which is made of copper. The magnetic field arising from the input ac signal will penetrate the thin film too. When the film becomes superconducting, any internal magnetic field is expelled. The thickness of copper on a PCB is about 13 micron, therefore, when the magnetic field increases outside the thin film, given its close contact, it is bound to influence the reflected ac signal from the microstrip.

A TiPd thin film was pasted face down on a **PCB** using GE Varnish (a low-temperature insulating adhesive). The **PCB** had a microstrip printed on it with

one end connected to the ground via a $50\ \Omega$ surface mount resistor and the other end can be connected to an input probe that we can use to send in an AC signal.

The **PCB** is made via optical lithography (using a solid PMMA layer as photoresist and exposing it to UV light under a microstrip mask) and wet etching (Copper etches in FeCl_3). It must be ensured that there is no shorting in the circuit on the **PCB**. The GE varnish layer must not be very thick and proper precautions must be taken while handling it because it is carcinogenic.

Much like the previous section, this **PCB** was mounted in a dilution refrigerator with one end connected to an input probe coming in from a lock-in amplifier which sends the RF signal. The same cable carries the reflected signal back which is fed into the lock-in after separating from the input signal using a directional coupler.

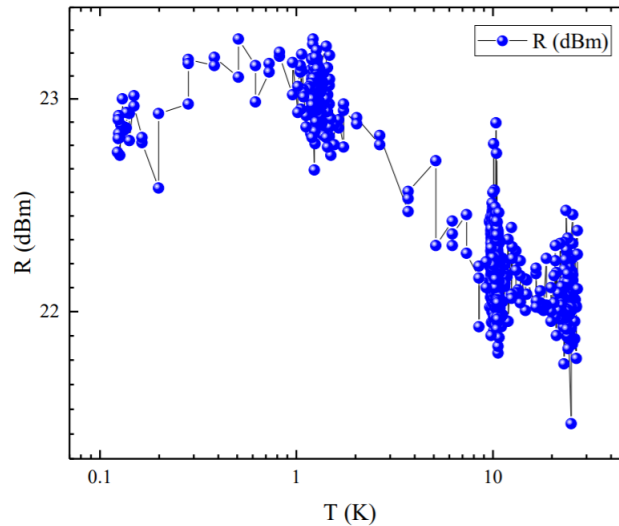


Figure 4.5: Reflected signal (in dBm) for microstrip in close contact with a superconductivity thin film measured at 2.35 MHz.

4.3 Theory

The section below will discuss the theory behind Meissner effect, which is the main principle behind both measurements described here, using London's equation. The second section will discuss magnetic field from a current carrying transmission line coupling to a thin film and effects on transmission and S parameters when the film becomes superconducting.

4.3.1 Theory of Diamagnetism in Superconductors

When a superconductor is cooled to below its transition temperature, it will expel all magnetic flux passing through it. If a flux is present in the material before transition to superconductivity, that field will be expelled below T_c . This phenomenon is called perfect diamagnetism. This is accomplished by shielding currents running on the surface of the superconductor, which cancel any magnetic field inside the superconductor up to a limit. Beyond a critical field value, we might observe a loss of superconductivity altogether (type I superconductors) or a mixed state with magnetic flux vortices running across the superconductor (type II superconductors).

Meissner effect was first observed by Meissner and Ochsenfeld. They indirectly measured that all internal fields have been canceled by measuring magnetic field very close to the surface of a superconductor below its transition temperature. When a superconductor expels magnetic field from the inside, it increases the magnetic field close to the surface. This is similar to what we try to observe in our microstrip experiment. London equations gave a phenomenological explanation for the Meissner effect.

In the Drude model of conductivity for finite frequency electric fields, the relation between electric field (E) and current density (j) is given as

$$j(\omega)e^{-i\omega t} = \sigma(\omega)Ee^{-i\omega t}$$

where the real part corresponds to currents in phase with the electric field applied and imaginary part for currents that are out of phase. The conductivity for the case of finite frequency turns out to be

$$\sigma(\omega) = \frac{ne^2}{m} \frac{1}{\tau^{-1} - i\omega}$$

For a perfect conductor, since there is no electron scattering, $\tau^{-1} \rightarrow 0$. Therefore,

$$\sigma(\omega) = -\frac{ne^2}{i\omega m}$$

Now, taking a curl of the equation $\mathbf{j} = \sigma\mathbf{E}$, we get

$$\begin{aligned}
(\nabla \times \mathbf{j})e^{-i\omega t} &= \sigma(\omega)(\nabla \times \mathbf{E})e^{-i\omega t} \\
&= -\sigma(\omega) \frac{d(\mathbf{B}e^{-i\omega t})}{dt} \\
&= i\omega\sigma(\omega)\mathbf{B}e^{-i\omega t} \\
&= \frac{ne^2}{m_e}\mathbf{B}e^{-i\omega t}
\end{aligned}$$

where, we have used the expression for conductivity given above. For $\omega \rightarrow 0$, we get the familiar London equation,

$$\nabla \times \mathbf{j} = \frac{ne^2}{m_e}\mathbf{B}$$

We also have Ampere's Law relating current density and magnetic field as

$$\nabla \times \mathbf{B} = \mu_0 \mathbf{j}$$

Combining the above two equations, we get

$$\nabla \times (\nabla \times \mathbf{B}) = -\mu_0 \frac{ne^2}{m_e}\mathbf{B}$$

or

$$\nabla \times (\nabla \times \mathbf{B}) = -\frac{1}{\lambda_L^2}\mathbf{B}$$

where λ_L is called the penetration depth. λ_L is the depth up to which magnetic field can penetrate a superconductor, beyond which it is less than $1/e$ times the external field and declines exponentially.

The above proof of the London equations shows that magnetic field is indeed expelled from a superconductor. This leads to an increase in the magnetic field outside the superconductor due to shielding currents on the superconductor's surface. In the microstrip experiment, when a thin film is placed in close contact with an ac current-carrying copper microstrip, magnetic field is expected to pass through the thin film. It is expected that if the thin film transitions to superconductivity, it will expel the magnetic field inside the superconductor, changing the reflected signal. Magnetic field expulsion leads to free energy minimization, therefore, the superconductor can sustain shielding currents.

4.3.2 Transmission Line and Magnetic Coupling

A transmission line can be modeled as an infinite series of inductors with capacitors connected to the ground after each inductor, as shown in the figure. A microstrip has two ports, therefore, we get a 2×2 S matrix. For a transmission line, the S parameters can be easily calculated if the input and output voltage values are known

$$S_{ij} = \left. \frac{V_i^-}{V_j^+} \right|_{V_k^+ = 0 \forall k \neq j}$$

where V_j^- is the reflected voltage at port j and V_j^+ is the input voltage at port j. The above methods measure the reflected coefficient from the one port which is known as an S_{11} measurement. Once the S matrix is known in a two-port microstrip, its input impedance can be calculated from the matrix elements.

$$(S) = \frac{1}{D_S} \begin{pmatrix} (Z^2 - Z_0^2) \sinh \gamma l & 2 \times Z \times Z_0 \\ 2 \times Z \times Z_0 & (Z^2 - Z_0^2) \sinh \gamma l \end{pmatrix}$$

where, $D_S = 2 \times Z \times Z_0 \cosh \gamma l + (Z^2 + Z_0^2) \sinh \gamma l$, Z_0 is characteristic impedance, Z is input impedance and γ is propagation constant. From the above set of equations, we can write

$$Z^2 = Z_0^2 \frac{(1 + S_{11})^2 - S_{21}^2}{(1 - S_{11})^2 - S_{21}^2}$$

and

$$e^{-\gamma l} = \left\{ \frac{1 - S_{11}^2 + S_{21}^2}{2S_{21}} \pm K \right\}^{-1}$$

$$K = \left\{ \frac{(S_{11}^2 - S_{21}^2 + 1)^2 - (2S_{11})^2}{2S_{21}^2} \right\}^{1/2}$$

The above equations for Z and γ give us the values of R, L, C and G parameters of the transmission line in terms of scattering parameters. Conversely, if the R, L, C and G parameters are known, we can derive an expression for each scattering matrix element. In the microstrip samples, the transmission line carrying the ac current is in close contact with the TiPd thin film, only separated by a thin insulating layer of GE Varnish. Therefore, we expect the magnetic field generated due to the ac signal to pass through the thin film too. Now, if the thin film becomes superconducting, it will expel any magnetic field through it by generating shielding currents on its surface which cancel magnetic field on the inside and increase magnetic field outside. This can be modeled as an inductor coupled to the transmission line and the Telegrapher's equation will include an extra mutual inductance term (we assume current is traveling in x-direction

and lossless transmission line)

$$-\frac{\partial V}{\partial x} = L \frac{\partial I}{\partial t} + L_M \frac{\partial I_{shield}}{\partial t}$$

and

$$-\frac{\partial I}{\partial x} = C \frac{\partial V}{\partial t}$$

where, V is the voltage across transmission line, I is the current through it and I_{shield} is the shielding current in the superconducting thin film, L is the inductance of the transmission line and L_M is the mutual inductance between the microstrip transmission line and superconducting thin film. The effective inductance in the system has changed, leading to a change in the voltage when the thin film becomes superconducting. This will lead to a change in S-matrix elements. Since S_{11} is measured in the experiment, we observe a change in the reflected signal.

The shielding current has to be at the same frequency as the current in the transmission line and taking both L_M and I_{shield} to be constant, we can simplify the Telegrapher's equations by taking ansatz for coupled equations

$$V = V^+ e^{-\omega \sqrt{LC}} + V^- e^{+\omega \sqrt{LC}}$$

and

$$I = \frac{1}{Z_0} \left(V^+ e^{-\omega \sqrt{LC}} + V^- e^{+\omega \sqrt{LC}} \right)$$

The new expression for Telegrapher's equation, including magnetic field coupling with a superconducting thin film can be written as

$$-\frac{\partial V}{\partial x} = \iota \omega (LI + L_M I_{shield})$$

and

$$-\frac{\partial I}{\partial x} = \iota \omega CV$$

Taking a second derivative to the first Telegrapher's equation, we get the exponential solution form for V and I , thus validating the ansatz used above

$$-\frac{\partial^2 V}{\partial x^2} = -\omega^2 LCV$$

and

$$-\frac{\partial^2 I}{\partial x^2} = -\omega^2 LCI$$

The shielding current in the superconductor must be in the opposite direction to the current in the microstrip which is the I^+ component. This means that I_{shield} will contribute to I^- and hence, to V^- which is the voltage of the reflected signal. Therefore, we expect an increase in the reflected signal and

$$V^- = \int -i\omega(LI^- + L_M I_{shield}) dx$$

and the $S_{11} = \frac{V^-}{V^+}$ parameter measured will increase because of an additional positive term in the numerator. However, this increase will be much smaller than the increase due to complete reflection of input signal as seen in the quartz crystal method. λ_L is least at absolute zero, $T = 0K$. Therefore, as the temperature is reduced, we would expect a decrease in penetration depth which will be achieved by an increase in the number density of the current-carrying electrons ($\lambda_L \propto \frac{1}{n}$), which is just an increase in the shielding current. This means the reflected signal (V^-) will increase as the temperature decreases.

4.4 Comparing the two methods

Using a quartz crystal is much better than using a microstrip because the microstrip method uses weak indirect effects which are harder to detect. This could lead to an error in T_C value. If the superconductor is not placed close enough to the copper layer, we might not observe a change in the reflected signal and wrongly conclude that there is no superconductivity in the fabricated film. The thin film is in direct contact with the input probe and current runs through the film to go between the two electrodes in the quartz crystal. In the microstrip method, there is no direct contact with the thin film. Two improvements are suggested for the microstrip method, one is using a meander geometry instead of a microstrip to capture distortion in reflected ac signal if the film pasted on top is indeed superconducting, and two, trying to create contacts on the thin film sample itself so that instead of capturing a distortion, a significant increase in the reflected signal is observed upon transition to superconductivity. However, making contacts on thin films is tricky and can come off after putting in the dilution fridge leading to no measurement at all. With a quartz crystal, we can try to couple the resonant vibration frequency of the crystal with the frequency of input ac signal to couple crystal vibrations to the electromagnetic wave which will give us more precise measurements. This measurement was not made in the current experiment since we got the results for 2.35 MHz, but this approach can be considered in future experiments with proper adjustments for good thermal conductivity since GE Varnish will curb crystal oscillation.

Chapter 5

Review and Future Work

5.1 Superconducting Nanowire Single Photon Detector (SNSPD): Experimental guide

In section 1.3, we have discussed the theory and working of Superconducting Nanowire Single Photon Detectors. Now, in order to make these devices, certain experimental parameters need to be set. A resistive hotspot is created after a photon is absorbed and this hotspot spreads in a spherical front within the nanowire. Although the hotspot formed has a radius between 25-50 nm depending on the photon's energy, to ensure efficient energy transfer between the phonon system of the superconductor and phonons in the substrate, the thickness of the thin film used to make the device must be below 10 nm. This allows for quick resetting time for the device.

Many crystalline materials like NbN, NbTiN, etc., which have higher transition temperatures, have been used to make SNSPD devices. It is this crystalline structure that leads to inferior device performance. The films we need to make our devices are very thin. Therefore, the superconducting properties of these films will strongly correlate with the properties of the substrate we choose. Even if a uniform substrate is chosen, if the film's crystalline structure does not match with the substrate's crystalline structure, there will be non-uniformities throughout the film and superconducting properties of the film will be suppressed. The limitations on substrate choice also lead to problems in device integration in complex waveguide circuits and optical cavities. Amorphous films like MoSi, MoGe and WSi_x have shown competing photodetection properties in thin film form and they don't have any strict substrate limitations which makes them an attractive alternative. In addition, MoGe shows a significantly smaller (less than half) superconducting energy gap than NbN which increases detection efficiency. It also shows higher T_c than its amorphous counterpart WSi_x making it less ex-

pensive to use and easier to manage in experiments. It might be tempting to consider high T_c materials for photodetection devices. These superconductors, however, possess a very large superconducting energy gap which makes the detection efficiency very poor.

The **SNSPD** device needs to be fabricated using electron beam lithography. The film is coated with an electron beam resist (PMMA A2 or A4) on which the electrons will pattern the device. The resist is spin-coated by running the spin coater program for 45 s - 1 min at 4000 rpm. After this, the sample is heated on a hotplate at 180 C for 1 min and 30 sec to get a uniform thickness of between 100 - 110 nm. The film must then be coated with an adhesive layer like titanium (~ 15 nm) followed by a 75 nm layer of gold or silver, which are good conductors and help prevent charge accumulation from e-beam exposure. It is a good idea to scratch one corner of the substrate before putting in **SEM** which helps in focusing. Xenos XPG2 is a device used for precise beam exposure control. A meander geometry pattern can be created using Xenos pattern generator. After marking the area on the substrate where the device will be patterned, select an origin corresponding to the origin written in the device pattern code. The current, exposure time and acceleration voltage must be optimised for different nanowire thicknesses. The nanowires must be uniform throughout the device to get a small range of critical current, otherwise, the device will not work. The exposed resist is developed in PG remover following which, reactive ion etching can be used to etch the pattern in MoGe thin film. The resist, Ti and Au/Ag layers can be removed after the pattern is etched on MoGe. The uniformity of the final device can be checked by **SEM** imaging and critical current measurement (if the range of I_c is broad, the wires aren't uniformly wide). Previous experiments for MoGe based **SNSPDs** suggest the following dimensions for meander wires, 16 μm length of each branch with a width of 150 nm and a gap of 80 nm between consecutive branches. These values show critical current at 2.5 K in the range of 7 - 8 μA . We can expect these values only when the device is uniform. These experiments have been carried out by Verma et al. [VLV⁺14] and Archan Banerjee [Ban17]. These parameters might and most probably will be different for our samples, however, the above works give a good starting point for device fabrication. These values can be fine-tuned by trying different values.

A current meter can be used to provide bias current across the device. It is usually biased at 97% of the critical current. The device must be kept in a cryostat at a temperature between 1 - 2.5 K (the critical current will change accordingly). The sheet resistance of MoGe is larger than 50 Ω . SMA connectors can be used to connect the device in the cryostat with current meter and output reading circuit. The current meter is fed into a bias tee with the dc output used to create a constant bias V_b across the device and rf output connected to a 50 Ω resistor which acts as the shunt circuit. The reading circuit must consist of low

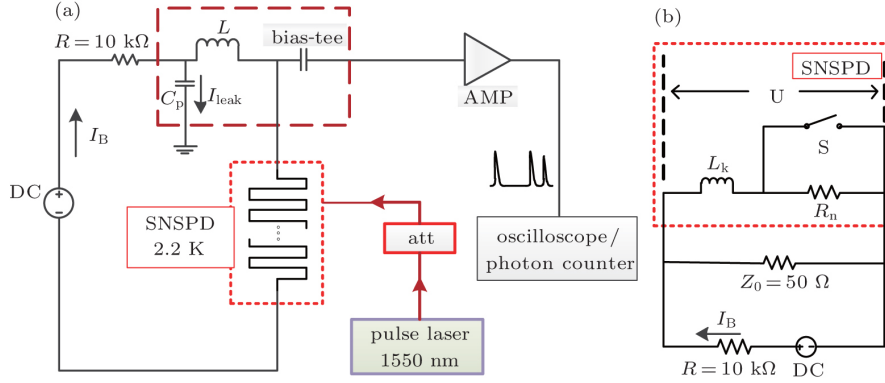


Figure 5.1: Circuit diagram for signal readout. The SNSPD is modeled as resistor and inductor in series. The bias tee values for capacitor and inductor are shown in the figure. The output pulse across the shunt resistor is amplified and recorded in an oscilloscope. Source [YHLWJ⁺15]

noise high-frequency amplifiers to amplify the pulse generated from a photon absorption event which is recorded in a wide spectrum oscilloscope. [Figure 5.1]

Usually, SNSPDs based on granular materials are faster, while those based on amorphous materials are more efficient. Future work on efficient SNSPDs can include a device made from a crystalline superconducting layer deposited over an amorphous superconductor layer with comparable critical current values such that proximity effect can carry the benefits of both films for superior photodetection devices. [ISB⁺17]

5.2 Vortex pinning experiments

Type II superconductors are characterised by the presence of an intermediate state between absolute superconductor and normal metal behavior. Such superconductors have two critical magnetic fields, above the first critical field value, the superconductor develops vortices that allow a quantum of flux (h/e) to pass through them. For applications like Superconducting Nanowire Single Photon Detector and electromagnets made from superconducting wires, a high current is required to pass through the superconductor. This current creates a magnetic field which leads to vortex formation above a certain value of the current. To maximize performance, both these devices are operated close to the critical current and studying vortex motion will help significantly in curbing its effects.

An exciting study in type II superconductors is that related to vortex pin-

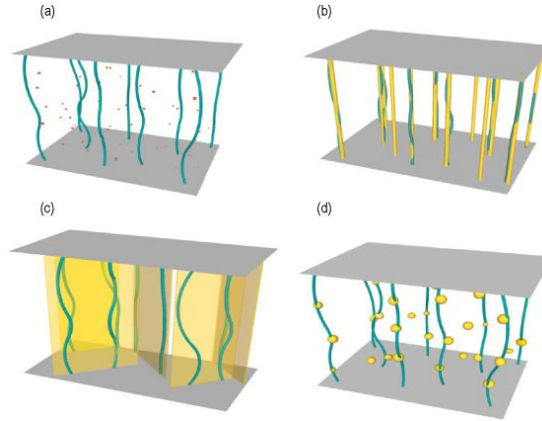


Figure 5.2: Schematic showing vortices running from the top of a superconductor to the bottom with flux pinned due to a) weak pinning centers, b) line defects, c) crystal boundaries, d) large pinning centers like foreign atoms, lattice irregularities or nanoparticles. [OPR⁺12]

ning. In the presence of a transverse current, the fluxoids (vortices) experience a Lorenz force that causes them to move and dissipate energy which can destroy superconductivity by creating a pseudo-resistance leading to a rapid increase in temperature. Movement of these vortices can lead to a reduced switching current (which is the observed current at which superconducting to normal transition happens and its value is typically smaller than the critical current) and a resistance tail which leads to a longer resetting time for superconducting devices like SNSPDs.

In order to increase the switching current, the fluxoids must be pinned in place using pinning centers. Defects (crystallographic irregularities or foreign atoms) in the superconductor lattice can act as pinning centers (Fig 5.2). Irradiating the sample with high-energy photons produces defects that can increase the superconductor's pinning potential. A crystalline material has grain boundaries that separate each continuous crystal from the next. These grain boundaries and defects can exert pinning force on a moving fluxoid which acts against the Lorenz force to keep it in place.

Bibliography

- [Ban17] Archan Banerjee. *Optimisation of superconducting thin film growth for next generation superconducting detector applications*. PhD thesis, University of Glasgow, 2017.
- [BBD⁺17] Archan Banerjee, Luke J Baker, Alastair Doye, Magnus Nord, Robert M Heath, Kleanthis Erotokritou, David Bosworth, Zoe H Barber, Ian MacLaren, and Robert H Hadfield. Characterisation of amorphous molybdenum silicide (mosi) superconducting thin films and nanowires. *Superconductor Science and Technology*, 30(8):084010, 2017.
- [Hug16a] Matt Hughes. Dc sputtering. <http://www.semicore.com/news/94-what-is-dc-sputtering>, 2016.
- [Hug16b] Matt Hughes. E-beam evaporation. <http://www.semicore.com/news/89-what-is-e-beam-evaporation>, 2016.
- [Hug16c] Matt Hughes. Rf sputtering. <http://www.semicore.com/news/92-what-is-rf-sputtering>, 2016.
- [Hug16d] Matt Hughes. Thermal evaporation. <http://www.semicore.com/news/71-thin-film-deposition-thermal-evaporation>, 2016.
- [Ins16] Excel Instruments. Sputtering gun. <https://www.excelinstruments.biz/sputter-source.php>, 2016.
- [ISB⁺17] Yachin Ivry, Jonathan J Surick, Maya Barzilay, Chung-Soo Kim, Faraz Najafi, Estelle Kalfon-Cohen, Andrew D Dane, and Karl K Berggren. Superconducting-superconducting hybridization for enhancing single-photon detection. *arXiv preprint arXiv:1703.08034*, 2017.
- [Kub88] Shugo Kubo. Superconducting properties of amorphous mox (x=si, ge) alloy films for abrikosov vortex memory. *Journal of applied physics*, 63(6):2033–2045, 1988.

- [LKHX10] Manlai Liang, Milind N Kunchur, Jiong Hua, and Zhili Xiao. Evaluating free flux flow in low-pinning molybdenum-germanium superconducting films. *Physical Review B*, 82(6):064502, 2010.
- [Ltd15] JEOL Ltd. Scanning electron microscope. <https://www.jeol.co.jp/en/science/sem.html>, 2015.
- [NTH12] Chandra M Natarajan, Michael G Tanner, and Robert H Hadfield. Superconducting nanowire single-photon detectors: physics and applications. *Superconductor science and technology*, 25(6):063001, 2012.
- [OPR⁺12] Xavier Obradors, T Puig, S Ricart, M Coll, J Gazquez, A Palau, and X Granados. Growth, nanostructure and vortex pinning in superconducting $\text{YBa}_2\text{Cu}_3\text{O}_{7-x}$ thin films based on trifluoroacetate solutions. *Superconductor Science and Technology*, 25(12):123001, 2012.
- [Pad18] Karmela Padavić. Cooper pair diagram. https://courses.physics.illinois.edu/phys498art/sp2018/PHYS489ART_SC_KP.pdf, 2018.
- [RDMMPPE20] C Reyes-Damián, F Morales, Esmeralda Martínez-Piñeiro, and Roberto Escudero. High-pressure effects on the intermetallic superconductor $\text{Ti}_{0.85}\text{Pd}_{0.15}$. *Journal of Superconductivity and Novel Magnetism*, 33(9):2601–2607, 2020.
- [Sci21] Thermo Fisher Scientific. Sem: Types of electrons and the information they provide. <https://www.thermofisher.com/blog/microscopy/sem-signal-types-electrons-and-the-information-they-provide/#:~:text=Secondary%20Electrons,-Unlike%20BSEs%20%20SEs&text=They%20are%20a%20result%20of%20inelastic%20interactions%20between%20the%20primary,topography%20of%20the%20sample's%20surface.>, 2021.
- [SSH⁺17] Mariia Sidorova, Alexej Semenov, Heinz-Wilhelm Hübers, Ilya Charaev, Artem Kuzmin, Steffen Doerner, and Michael Siegel. Physical mechanisms of timing jitter in photon detection by current-carrying superconducting nanowires. *Physical Review B*, 96(18):184504, 2017.
- [Ste06] Gary Alexander Steele. *Imaging transport resonances in the quantum Hall effect*. PhD thesis, 2006.

- [uce03] ucerkb. Sputtering. http://users.wfu.edu/ucerkb/Nan242/L07-Sputtering_a.pdf, May 2003.
- [VLV⁺14] Varun B Verma, Adriana E Lita, Michael R Vissers, Francesco Marsili, David P Pappas, Richard P Mirin, and Sae Woo Nam. Superconducting nanowire single photon detectors fabricated from an amorphous $\text{Mo}_0.75\text{Ge}_0.25$ thin film. *Applied Physics Letters*, 105(2):022602, 2014.
- [Wik21] Wikipedia. Capacitance meter. https://en.wikipedia.org/wiki/Capacitance_meter, 2021.
- [YHLWJ⁺15] He Yu-Hao, Chao-Lin Lü, Zhang Wei-Jun, Zhang Lu, Wu Jun-Jie, Chen Si-Jing, You Li-Xing, and Wang Zhen. Statistical analysis of the temporal single-photon response of superconducting nanowire single photon detection. *Chinese Physics B*, 24(6):060303, 2015.
- [YKD⁺07] Joel KW Yang, Andrew J Kerman, Eric A Dauler, Vikas Anant, Kristine M Rosfjord, and Karl K Berggren. Modeling the electrical and thermal response of superconducting nanowire single-photon detectors. *IEEE transactions on applied superconductivity*, 17(2):581–585, 2007.

Appendix A: Growth of Capacitor for Magnetocapacitance Studies

A.1 Fabrication of Nickel thin film capacitors

The aim was to create a parallel plate capacitor with one of the plates susceptible to change in properties in the presence of a magnetic field. This would create a change in the electric field in the dielectric and change the capacitance of the capacitor. This phenomenon is called magnetocapacitance. The study of magnetocapacitance is important for its applications in compact memory storage devices since memory can be stored through both electric and magnetic polarization providing two degrees of freedom. These devices are also used in microwave filters, magnetic field sensors etc.

For this purpose, an n-doped silicon substrate with 285 nm silicon oxide layer deposited on it obtained from Graphene Laboratories Inc. was used. The n-doped silicon is highly conducting with a resistivity of $\sim 0.005 \Omega$ and acts as one of the conducting plates. The silicon oxide layer acts as the dielectric between the plates. $1 \text{ cm} \times 1 \text{ cm}$ chips were cut out for making the capacitor.

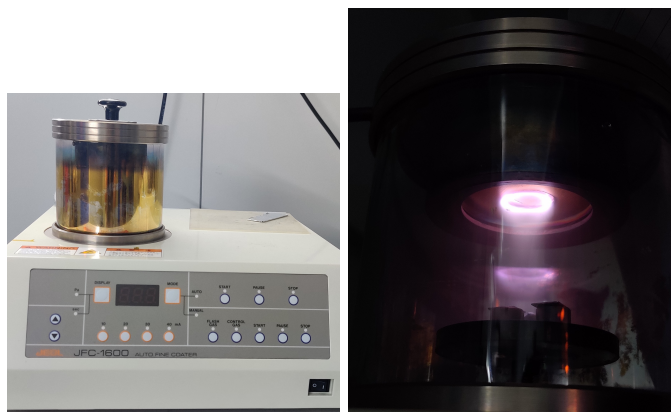
A.1.1 Pre-treatment

The n-doped silicon substrate was cleaned to remove any wafer dust that might have stuck to the wafer after cutting and to remove the PMMA coating on top which prevents scratching. We needed to create a contact on the conducting silicon wafer (we will call this the back contact due to its position on the PCB while making contacts for capacitance measurement).

The back side of the wafer is not conducting due to silicon oxide layer since silicon exposed to air will oxidise and form a thin layer of silicon oxide. In order to make the back contact, the back layer of silicon oxide (not the dielectric layer) needs to be scratched. A diamond cutter was used to scratch the back while regularly checking the resistance between two points. The back has a dull

appearance initially which starts to appear shiny after scratching. Care should be taken to not scratch too hard, use a light hand and go in zigzag motions repeatedly over most of the back surface. Scratching too hard could lead to chipping on the edges of the chip, which can lead to shorting when the capacitor is made or, a crack in the chip which will make it unusable.

The resistance between two points roughly 1 cm apart will be in the range $20\ \Omega$ - $80\ \Omega$ after scratching. The chip is cleaned again using the cleaning procedure to remove the dust created from scratching which might stick to the chip. To ensure the back side remains conducting and an oxide layer doesn't form on it again, gold is sputtered on the back side. This is done using the JEOL JFC-1600 Auto Fine Coater. Setting the current at 40 mA, the pressure is reduced to about 7 Torr at which point the plasma is created and gold is deposited for 120 seconds.



(a) JEOL JFC-1600 Auto Fine Coater used for gold sputtering. (b) Plasma visible in the sputtering chamber.

A.1.2 Depositing Nickel

Nickel thin film acts as the top plate for the capacitor and thermal evaporation is used for depositing the nickel. The thermal setup consists of three sets of two stages each and across one set, a boat made of molybdenum is connected. Nickel pellets are put in a depression on the boat. The sample is placed inverted on the top with a shutter which can be rotated. The chamber is kept in a vacuum of about 4×10^{-6} Torr. A good vacuum is required to avoid oxidation of nickel as it evaporates.

When current is passed across the boat, due to joules heating, the boat heats up and in the process heats the nickel pellets on it. Nickel evaporates and gets

deposited on the sample when we open the shutter and also on the **Quartz Crystal Microbalance (QCM)** which is used to determine the thickness as nickel is being deposited and we can control the thickness of our film precisely. The rate of evaporation must be kept roughly constant (1 Å-1.5 Å) to maintain even deposition.

The current supplied to the boat must be increased very slowly (it should take about 15 minutes to get to nickel's evaporation) and preferably slower when the boat becomes red hot because the boat expands as it gets hot which leads to axial stress due to confinement on the two ends. Too much stress can cause the boat to break. A slow increase in current also ensures nickel obtains an even rate of evaporation because if the boat gets too hot, it could lead to flash evaporation of the pellets evaporating off most of the nickel before the shutters are even opened. The current should be decreased slowly because the boat is contracting and a sudden decrease in its temperature could create stress which could cause the boat to break in the next evaporation. It should also be ensured that only boats specified for nickel evaporation be used to avoid contamination of other elements. To get a film thickness of 100 nm or lower, two pellets are enough. Putting more than three pellets on the boat would also lead to strain and potential boat breakage. Putting the system in vacuum takes about 6-7 hours therefore, to save time in case a boat breaks mid-deposition, a back-up boat should be kept in the chamber. If a second boat is used for deposition, the tooling factor for **QCM** and the sample holder position must also be changed. Before changing the knob of current supply, which redirects the current supplied to the second boat, bring down the current to zero, turn off the current supplier from the main switch and then change the knob.

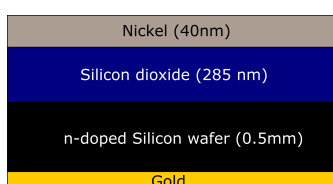


Figure 4: *The thin film capacitor device. All the layers are shown here.*

A.2 Making the PCB and contacts

Connections on a thin film device are different from the regular capacitors and resistors which have wires to connect to a circuit. These devices need a **PCB** on which we can connect the two plates of the capacitor and connect the pcb to a breakout box for connection to any circuit. The **PCB** was made by sketching on



Figure 5: A PCB with sketched arms made for measuring resistance between the two plates of a thin film capacitor.

a copper plated board (which had a $13\ \mu\text{m}$ copper layer on top of a thermally conducting dielectric) using an anti-etching marker and then etching the rest of the copper in FeCl_3 (process explained in section ??). The sketched PCB can be seen in Fig 5. The section in the center is connected to one arm and all other arms are insulated from the central copper section and from each other. This was confirmed using a multimeter.

To make a contact of the back plate (which is coated with gold) with the PCB, half of the back plate is pasted to the copper using GC varnish and the other half is covered with indium paste which is conducting thus giving us a contact with the back plate. For top contact, a gold wire is used because of its high conductivity. The wire is coated with indium solder on one end and the other end is soldered to a conducting arm on the PCB, again, using indium solder. Indium solder is used because it has a lower melting point which prevents the thin gold wire from breaking due to overheating. The indium coated end is pressed on the top plate of the capacitor using a thin wooden stick covered with thread seal tape to avoid scratching the device. Pressing the indium coated end flattens indium onto a surface (Fig 6) because of its soft texture which gives good adhesion to the nickel film. To check if the wire is properly connected on both ends, tug at it gently.

Once connections to the PCB are made, the arms of the PCB are connected to a D-subminiature connector (DE-9) which is connected to a breakout box. The appropriate bnc connectors on the breakout box are used to connect out device to any circuit as required. The setup can be seen in Fig 7.

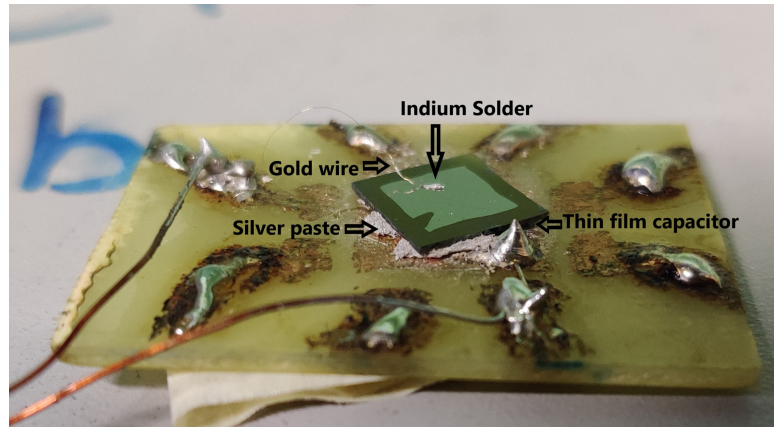


Figure 6: Thin film capacitor with top contact of gold wire attached via indium solder.

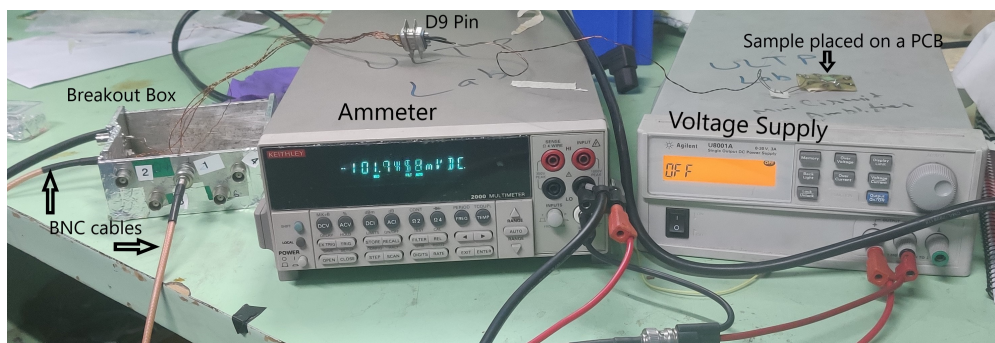


Figure 7: The setup used to measure resistance between the top and bottom plates of fabricated capacitors. Keithley 2000 multimeter is used as the ammeter; Agilent UB001A DC power supply is used to create a voltage between the two plates of capacitor.

A.3 Challenges

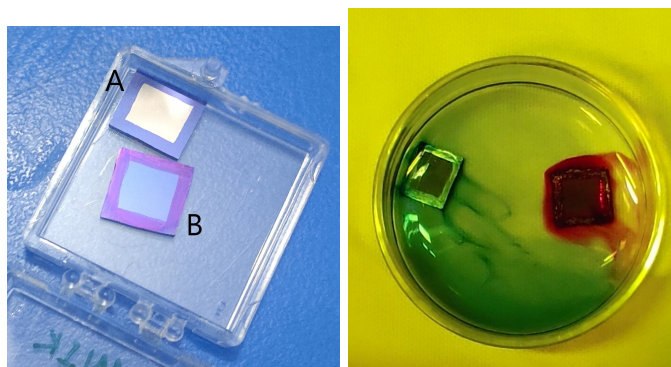
The initial few capacitors were all shorting, the resistance between the top and bottom plates was of the order of a few hundred ohms. Ideally, the resistance should be in Megaohms or more. It was deduced that this might be occurring due to gold or nickel (or both) depositing over the edges and coming in direct contact with the plate contact on the other side. To solve this issue, two ideas were proposed, we could either cut the capacitor on all sides after depositing as earlier, or, we could coat all the edges with paint before deposition which can be taken off without affecting the capacitor after deposition.

In addition to this, making a good contact with the back plate is important. The plate was initially connected to the **PCB** using indium paste and GC varnish but it wasn't a good conducting contact. Copper tape too didn't make a good contact with the device because the tape gets deformed very easily and doesn't stick to a large enough surface area of the capacitor back plate.

A.4 Steps to overcome the challenges

In order to ensure the top and bottom plates do not come in contact, the edges were painted. The vertical edges and the edges of the top and bottom contacts were painted using an anti-etching marker and another samples was painted using black nail paint. Application of the marker was much easy and more precise compared to the nail paint. The marker also dries very quickly whereas the nail paint takes around ten minutes to dry.

After the chips are cleaned, they are scratched in the back so that when gold is sputtered on the back, it has contact with the n-doped silicon. The chips are then cleaned again to get rid of any dust particles resulting from scratching that might stick to the chip. They are then painted (as seen in the figure: only painted chips). The deposition of gold and nickel follows as explained above. The paint - both the marker and nail paint - are easily removed by putting the chips in isopropyl alcohol (IPA) for five minutes, gently rubbing all the edges with a soft bristle paint brush and then blow drying. This does not affect the rest of the deposited nickel or gold film in the central part of the top and bottom faces.



(a) A: Chip with deposited nickel in the center and no deposition on and near the edges. B: Chip with edges painted using antietching marker. **(b)** Cleaning marker and nailpaint from chips using IPA.

A.5 DC measurement

Resistance measurements were made between the two plates of the capacitor using dc signal. Initial measurement was made by using copper tape as bottom contact and multimeter pin in direct contact with the top plate. This measurement showed resistance in the megaohms range. These measurements were then verified using the setup in figure 7. Voltage in the range 10 mV to 200mV was applied between the two plates, values above this can harm the capacitor device. The background current measured in the absence of applied voltage is $1.7 \times 10^{-7} A$. For the above range of applied voltage, the current barely fluctuated from the base current. This showed that the resistance between the capacitor plates is at least of the order of a few Megaohms.

The methods used to avoid shorting in the thin film capacitors seem to have worked and all this technique can be used to make further samples. One of the easiest methods of measuring a capacitance is through a digital voltmeter. These typically have a range of measurement between nanfarad and microfarad. They measure the capacitance by charging the capacitor and discharging it with a known amount of current and measuring the time taken for the voltage to increase and decrease. Another method of measuring capacitance is by passing alternating current across the capacitor and measuring the resulting voltage. This measurement too has a range of nanofarads to microfarads. The precision of capacitance measurement can be increased by using bridge circuits which work much like a resistance bridge except one of the resistors is replaced with a variable capacitor and a balancing condition is enforced to find the capacitance of the capacitor under test.

A rough estimate of the capacitance of the fabricated thin film capacitor can be made as

$$C = \frac{\epsilon_r \epsilon_0 (Fm^{-1}) A(m^2)}{d(m)}$$

A silicon dioxide ($\epsilon_r = 3.7$) layer 285 nm thick acts as the dielectric and the approximate area of the plates is 0.5 cm \times 0.5 cm each. Therefore,

$$C_{estimate}(Farads) = \frac{3.7 \times (8.85 \times 10^{-12}) \times (0.005 \times 0.005)}{285 \times 10^{-9}} \sim 2.5 \times 10^{-9} F$$

For this measurement, we need a sensitive measurement device to measure the capacitance accurately. The capacitance of this device changes in the order of attofarads which requires even more sensitive measurement. A capacitance bridge can be used in such cases and this is discussed in the next section.

A.6 Capacitance measurement

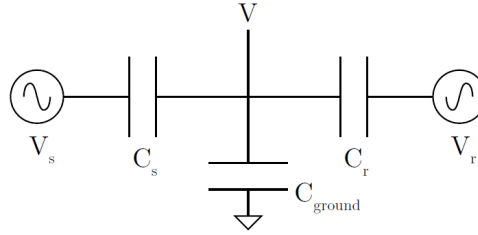


Figure 9: The circuit of a capacitance bridge used to measuring capacitance. Source [Ste06]

Capacitance can be measured using a capacitance bridge as shown in Fig 9. The capacitor C_r is accurately known and taken as reference. There is always stray capacitance due to the wires and other connections which can all be clubbed under one ground capacitance term C_g . Therefore, the equation for this bridge is given as:

$$C_T V = C_S V_S + C_r V_r$$

where the term $C_T = C_S + C_r + C_g$.

In order to measure the capacitance of the sample capacitor accurately, the reference voltage V_r must be 180° out of phase to V_S such that the voltage at the center of the bridge V is zero. This greatly simplifies the equation above and we get an expression for sample capacitance

$$C_S = \frac{C_r V_r}{V_S}$$

A major advantage of this method is accurate measurement of small capacitance without the requirement to measure stray capacitance to the ground. Moreover, since the voltage in the center of the bridge has been made zero by selection, V does not come in the calculation and gain or noise from an amplifier does not reduce accuracy of the measurement. This bridge can also be used to detect change in capacitance when a balanced bridge is placed in a magnetic field. We can vary either the reference capacitor and redo the calculation above to obtain change in capacitance or we can vary the reference voltage V_r to get $V = 0$ and then find the change in capacitance by comparing previously obtained value with this one. This work constitutes future direction for the work on magnetocapacitance.

Many commercial capacitance bridge meters are available for precise mea-

surement of capacitance like the Andeen-Hagerling 2700A capacitance bridge which has variable impedance in all other branches of the bridge which can be adjusted to balance the bridge. Using four-probe connections and precisely known variable impedance values, these bridges can measure capacitance of the order of a few farads all the way down to picofarads. [Wik21]